ADVANCES IN ATMOSPHERIC SCIENCES, 2022

• **Original Paper** •

Influence of Coastal Marine Boundary Layer Jets on Rainfall in South China※

Yu DU*[1,2,3], Yian SHEN[4], and Guixing CHEN[1,2,3]

[1]*School of Atmospheric Sciences, Sun Yat-sen University, and Southern Marine Science and Engineering Guangdong Laboratory (Zhuhai), Zhuhai* 519082, *China*

[2]*Guangdong Province Key Laboratory for Climate Change and Natural Disaster Studies, Sun Yat-sen University, Zhuhai* 519082, *China*

[3]*Key Laboratory of Tropical Atmosphere-Ocean System (Sun Yat-sen University), Ministry of Education, Zhuhai* 519082, *China*

[4]*Huzhou Meteorological Bureau, Huzhou* 313000, *China*

(Received 27 May 2021; revised 27 July 2021; accepted 24 August 2021)

ABSTRACT

Coastal marine boundary layer jets (CMBLJs) play an important role in coastal and inland rainfall in South China. Using 21 years of ERA5 and CMORPH rainfall data, two main CMBLJs are found, one on each side of Hainan Island (named BLJ-WEST and BLJ-EAST), which are always strengthened jointly. Both CMBLJs often occur in the pre-summer rainy season and exhibit an evident diurnal cycle with a maximum at night. With the emergence of the CMBLJs, rainfall is significantly enhanced in South China, particularly downstream of each CMBLJ. The response of rainfall to the CMBLJs is mainly attributed to convergence at the terminus of each CMBLJ, terrain-induced lifting, and relevant atmospheric stratification. Coastal rainfall downstream of the BLJ-WEST is much weaker than that downstream of the BLJ-EAST because of higher CIN over the Beibu Gulf, which is caused by lower temperature lapse rates and adiabatic heating in the lee of the Annamite Range. The inland rainfall increases along with CMBLJ intensity, whereas coastal rainfall reaches a maximum in the presence of moderate CMBLJs rather than stronger CMBLJs. Stronger CMBLJs induce stronger dynamic lifting but higher CIN near the coastal area. Additionally, CAPE near the coast does not become highest with strongest CMBLJs, because the CAPE generation contributed by coastal dynamic lifting can be offset by the negative contribution caused by the horizontal advection of cold and dry air from the Indochina Peninsula. Therefore, anomalous dynamic lifting, moisture flux convergence, and CAPE/CIN associated with CMBLJ intensity jointly result in anomalous rainfall.

Key words: low-level jet, rainfall, CAPE, CIN, coastal region

Citation: Du, Y., Y. A. Shen, and G. X. Chen, 2022: Influence of coastal marine boundary layer jets on rainfall in South China.. *Adv. Atmos. Sci.*, https://doi.org/10.1007/s00376-021-1195-7.

Article Highlights:

- Two CMBLJs, one on each side of Hainan Island, are observed in the pre-summer rainy season and exhibit a diurnal cycle with a maximum at night.
- Coastal rainfall downstream of the BLJ-WEST is much weaker than that downstream of the BLJ-EAST because of higher CIN over the Beibu Gulf.
- Inland rainfall increases along with CMBLJ intensity, whereas coastal rainfall does not reach a maximum that corresponds with strongest CMBLJs.

1. Introduction

Low-level jets (LLJs) are regarded as an important factor regulating the intensity and distribution of rainfall (Stensrud, 1996; Rife et al., 2010; Du and Chen, 2018, 2019a). LLJs typically can be classified into two types, including synoptic-system-related LLJs (SLLJ) and boundary

※ This paper is a contribution to the special issue on Predictability, Data Assimilation and Dynamics of High Impact Weather—In Memory of Dr. Fuqing ZHANG.

* Corresponding author: Yu DU
Email: duyu7@mail.sysu.edu.cn

layer jets (BLJ), both of which play distinct roles in rainfall owing to different characteristics and formation mechanisms (Chen et al., 1994; Du et al., 2014; Zhang and Meng, 2018; Du and Chen, 2019b).

Compared to SLLJs driven by synoptic disturbances, such as a low-pressure vortex or fronts, BLJs often occur next to mountains, like the Rocky Mountains (Bonner, 1968) and Andes Mountains (Marengo et al., 2004), or off coasts; some examples of coastal marine BLJs are the California coastal jet (Doubler et al., 2015), Chilean coastal jet (Garreaud and Muñoz, 2005), BLJ in Bohai (Zhang et al., 2018), and BLJ off the southeastern coast of China (Du et al., 2015). However, due to observational limitations, coastal marine BLJs (CMBLJs) have been studied less than BLJs over land, especially concerning their link to rainfall.

The formation mechanisms of the BLJs over land are explained by two main theories, including "Blackadar mechanism " (or called inertial oscillation theory, Blackadar, 1957) and "Holton mechanism" (thermal forcing over sloping terrain, Holton, 1967), or their combination (Du and Rotunno, 2014; Shapiro et al., 2016). Unlike the BLJs over land, CMBLJs occur in the absence of obvious diurnal eddy viscosity over the sea. Thus, the typical inertial oscillation mechanism caused by diurnal vertical mixing in the boundary layer does not work for CMBLJs. Du et al. (2015) revealed that inertial oscillation triggered by the thermal contrast between the land and ocean plays an important role in the CMBLJ off the southeast coast of China. Burk and Thompson (1996) suggested that the California coastal jet is also closely related to enhanced coastal baroclinicity. The diurnal variation of the baroclinicity along with inertial and friction effects can further affect the delay of the jet maximum in the early evening. In addition to baroclinicity, coastal terrain has an influence on CMBLJ intensity (Li and Chen, 1998; Chakraborty et al., 2009; Jiang et al., 2010; Chen et al., 2017b). For instance, the Somali jet is intensified by deflecting westerly low-level air northward due to the East African mountains acting as a western boundary (Krishnamurti et al., 1976).

Some previous studies have documented that CMBLJs can regulate rainfall near coasts via transporting moisture and providing convergence (e.g., Neiman et al., 2002; Du and Chen, 2019b), and their effects vary among regions. The California Landfalling Jets Experiment statistically links rainfall rates near the coastal mountains to the hourly upslope flow of the California coastal jet (Neiman et al., 2002; White et al., 2003), which is known as an atmospheric river because of transferring abundant water vapor (Smith et al., 2010). The Caribbean LLJ is found to coincide with a maximum in rainfall off the Caribbean coast of Nicaragua and Costa Rica (Amador et al., 2000; Whyte et al., 2008), while the strong West African westerly jet results in enhanced coastal rainfall through low-level moisture transports (Liu et al., 2020). In east Asia, a BLJ over the northern South China Sea (NSCS) horizontally transports moisture from the NSCS to Taiwan, favoring rainfall near the southwestern coast of Taiwan (Tu et al., 2019).

Over southern China, both SLLJs and BLJs are observed under variations in features (Du and Chen, 2019b, Li and Du, 2021). SLLJs generally occur over land, whereas BLJs prevail over the NSCS. SLLJs have been widely studied in terms of their formation mechanisms and their relationship with rainfall (Tao and Chen, 1987; Chen and Yu, 1988), however, BLJs and their impacts on rainfall are still not well understood. Du et al. (2014) exhibited two high-occurrence regions of CMBLJs over the Beibu Gulf and NSCS, which are both in proximity to the coast of South China and on either side of Hainan Island. Therefore, it is worth studying the detailed features of these two CMBLJs and their relationship with each other. Furthermore, since CMBLJs can induce convergence at their termini and interact with coastal terrain, as well as provide favorable thermodynamic conditions by transporting warm moist air, several questions arise: (1) What is the relationship between the intensity of the two CMBLJs and rainfall? (2) What is the relative importance of the dynamic and thermodynamic effects of the CMBLJs on rainfall?

The primary objective of the present study is to reveal how the two CMBLJs influence rainfall in south China dynamically and thermodynamically from a climatological point of view. The data and statistical methodology are briefly described in section 2. In section 3, we present the statistical characteristics of the two CMBLJs and their relationship with each other. Section 4 describes different rainfall patterns associated with the intensity of the two CMBLJs and further discusses their relevant dynamic and thermodynamic effects. The results of this study are summarized in section 5.

2. Data and Methodology

2.1. *Data used in this study*

The latest ECMWF atmospheric reanalysis, ERA5, is utilized to analyze the CMLLJs' activities and related atmospheric processes. ERA5 is the fifth generation of ECMWF atmospheric reanalysis of the global climate and follows ERA-Interim. Since ERA5 has high spatial and temporal resolution with a horizontal grid spacing of 0.25° × 0.25° and a time interval of 1 h, it has been widely used to identify low-level jets (Du and Chen, 2019b; Kalverla et al. 2019; Chen et al., 2021). Other datasets, like ERA-Interim, are also examined and show similar results but with lower resolution.

To display the precipitation distributions associated with the CMLLJs, we used Climate Prediction Center morphing technique (CMORPH) rainfall data (Joyce et al., 2004) with a temporal resolution of 30 min and a horizontal resolution of 8 km. CMORPH is derived by low-orbit satellite microwave data and geostationary infrared data. CMORPH data presents good performance in rainfall estimates and has been widely used in previous studies (Chen et al., 2018; Du and Chen, 2018). For consistency in temporal resolution and period coverage, both CMORPH rainfall data and

ERA5 data used in the present study cover from 1998 to 2018 and have a temporal resolution of 1 h.

2.2. *Criteria for identifying CMBLJ*

To identify the existence of a BLJ, the following criteria are adopted: (1) the maximum wind speed is more than 10 m s^{-1} within the lowest 100-hPa layer above the surface, (2) below 600 hPa, the wind speed must decrease by at least 3 m s^{-1} from the height of the wind maximum to the wind minimum above that, and (3) the meridional wind component at the jet vertical core is greater than zero. These criteria to identify a BLJ in East Asia have been widely used in previous studies (Du et al., 2014; Du and Chen, 2019a; Tu et al., 2019).

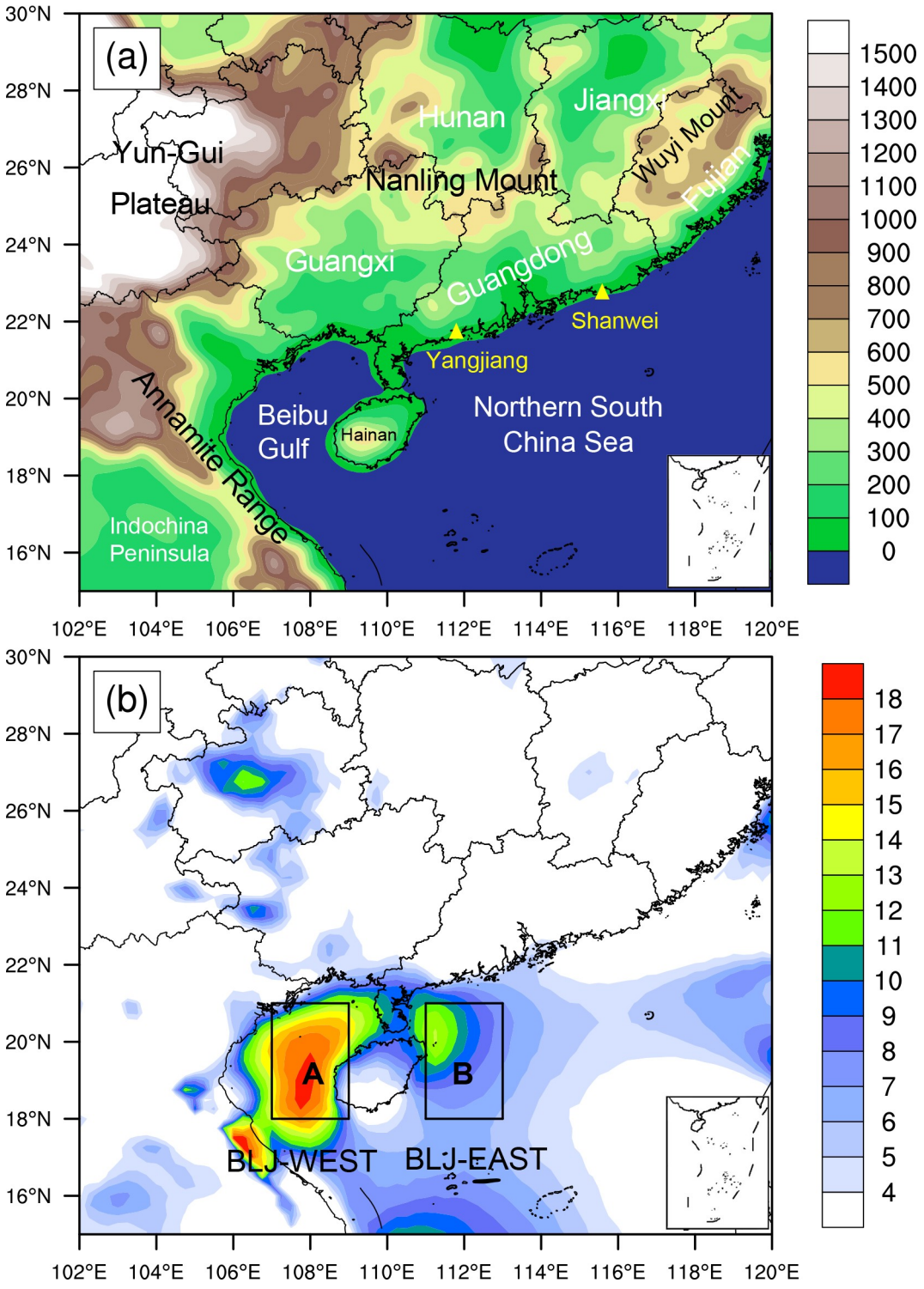

Fig. 1. (a) Terrain height (shading, m). (b) Distribution of BLJ occurrence frequency (shading, %). Boxes A and B are the regions selected for the BLJ-WEST and BLJ-EAST event definition, respectively.

Based on the high-occurrence region of BLJs (Fig. 1), we further classify CMBLJ events as occurring over the Beibu Gulf (BLJ-WEST) or NSCS (BLJ-EAST). BLJ-WEST and BLJ-EAST events are defined as when more than 50% of the grid points in boxes A and B of Fig. 1b satisfy the BLJ criteria, respectively. There is no requirement for the duration of the BLJ events, and the criteria of the BLJ events are hourly-based.

2.3. *Budget of CAPE generation*

The budget of convective available potential energy (CAPE) is calculated to investigate the influence of the CMBLJ on the change of CAPE distribution. The local change of CAPE can be written as (Emanuel, 1994; Zhang, 2002; Chen et al., 2014; Chen et al. 2017a):

$$\frac{\partial \mathrm{CAPE}}{\partial t} = \int_{p_{\mathrm{lnb}}}^{p_{\mathrm{sl}}} R_{\mathrm{d}}\left(\frac{\partial T_{\mathrm{v_p}}}{\partial t} - \frac{\partial T_{\mathrm{v_e}}}{\partial t}\right)\mathrm{d}(\ln p)$$
$$\approx c_p\left(T_{\mathrm{v_{sl}}} - T_{\mathrm{v_{lnb}}}\right)\frac{\partial \ln\theta_e}{\partial t} - \frac{\partial}{\partial t}\left(\phi_{\mathrm{lnb}} - \phi_{\mathrm{sl}}\right), \quad (1)$$

when the air parcel is lifted from the source level p_{sl} to the level of neutral buoyancy p_{lnb}. $T_{\mathrm{v_p}}$ and $T_{\mathrm{v_e}}$ are virtual temperatures of the air parcel and the environment aloft. $\phi_{\mathrm{lnb}} - \phi_{\mathrm{sl}}$ is the geopotential thickness of convection layer. R_{d} is gas constant of dry air, and p is pressure. Based on the method introduced by Chen et al. (2014), the local change of CAPE is linked to the boundary layer forcing $\mathrm{Term_{bl}} = c_p\left(T_{\mathrm{v_{sl}}} - T_{\mathrm{v_{lnb}}}\right)\partial \ln\theta_{\mathrm{e}}/\partial t$ and the free-atmospheric forcing $\mathrm{Term_{fa}} = -\partial/\partial t\left(\phi_{\mathrm{lnb}} - \phi_{\mathrm{sl}}\right)$.

Furthermore, the local change of the air parcel's equivalent potential temperature θ_{e} is given as follows:

$$\frac{\partial \theta_{\mathrm{e}}}{\partial t} = -u\frac{\partial \theta_{\mathrm{e}}}{\partial x} - v\frac{\partial \theta_{\mathrm{e}}}{\partial y} - w\frac{\partial \theta_{\mathrm{e}}}{\partial z} + Q, \quad (2)$$

which means the boundary layer forcing can be further divided into horizontal advection, vertical lifting, and external diabatic heating Q. Q is calculated as a residual. In addition to Q, the residual term also includes radiation effects, rainfall evaporation, and sub-grid processes like turbulence. The estimation errors of Q become large near the surface. So, the generation of convective instability by various processes due to LLJs can be calculated at a high accuracy using hourly data. The difference of $\partial \mathrm{CAPE}/\partial t$ and $\mathrm{Term_{bl}} + \mathrm{Term_{fa}}$ represents a calculation error of this budget estimate, which is relatively small in this case. In this way, we can quantitatively analyze the influence of the CMBLJ via the budget of CAPE.

3. Characteristics of the CMBLJs

3.1. *Structures and variations of the CMBLJs*

Before the influence of the CMBLJs on rainfall is elucidated, it is necessary to investigate their own characteristics, including spatial structures and temporal variations. Figure 1b shows the horizontal distribution of the occurrence frequency of BLJs during January–December 1998–2018. Two regions with high occurrences of BLJs are identified over the Beibu Gulf (around 19°N, 108°E, a maximum of ~18%) and over the NSCS (in proximity to the northeastern coast of Hainan, around 19.5°N, 111.5°E, a maximum of ~14%). Compared to the two high-incidence regions, BLJs rarely occur over land in South China. These two high-incidence CMBLJs on either side of Hainan Island are the BLJ-WEST and BLJ-EAST. The vertical distributions in occurrence frequency of the two CMBLJs show that both the BLJ-WEST and BLJ-EAST have peaks at 950 hPa (Fig. 2a). Compared to the BLJ-EAST, the BLJ-WEST occurs more frequently below 950 hPa.

As shown in Fig. 2b, the occurrence frequencies of the BLJ-WEST and BLJ-EAST events exhibit pronounced diurnal cycles with maximums at night (0200–0500 Local Standard Time, LST = UTC + 8). The peak in occurrence of the BLJ-WEST occurs ~2–3 h earlier than that of the BLJ-EAST. In addition, the diurnal cycle amplitude of the BLJ-WEST is larger than that of the BLJ-EAST. The diurnal cycle mechanism of the two CMBLJs has been discussed in previous studies (Du and Chen, 2019b; Kong et al., 2020). Kong et al. (2020) documented that the BLJ-WEST mainly occurs at night because the upstream wind strengthens and flows over the Annamite Range after sunset, which includes a hydraulic jump jet over the downstream of the mountain. Du and Chen (2019b) suggested that the nocturnal enhancement of the BLJ-EAST is caused by inertial oscillation coupled with large-scale land–sea breeze circulation. It is noted that a sharp decrease exists between 1700 and 1800 LST (and between 0500 and 0600 LST) in diurnal variation of the two CMBLJs because ERA5 uses 12-h windows of 4D-Var data assimilation (from 0900 UTC to 2100 UTC and 2100 UTC to 0900 UTC) (Chen et al., 2021).

Besides diurnal variations, the occurrence frequencies of the two CMBLJs exhibit pronounced seasonal variations with maximums in April–June, which is the early-summer rainy season in South China. Additionally, the BLJ-WEST events occur more frequently than the BLJ-EAST events (28% vs 15%) in the early-summer rainy season (Fig. 2c). Given the high occurrences of the CMBLJs and large precipitation in South China, we mainly focus on the early-summer rainy season in the remainder of this study.

Figure 3 presents the horizontal wind speeds at low levels averaged during the BLJ-WEST events and the BLJ-EAST events compared to those from the whole early-summer rainy season. During the BLJ-WEST or BLJ-EAST events, the southerly or southwesterly low-level winds near the coast of South China (~8–12 m $\mathrm{s^{-1}}$) are much stronger than those for the seasonal mean (~0–6 m $\mathrm{s^{-1}}$). In general, the locations of maximum winds are vertically tilted to the north (Fig. 3) due to the rise in terrain or stronger boundary layer mixing over the land. For instance, the 950-hPa southerly winds are centered in the Beibu Gulf and the NSCS (Figs. 3a, c, and e), whereas the 850-hPa southwesterly winds are greatest over land in southern China (Figs. 3b, d,

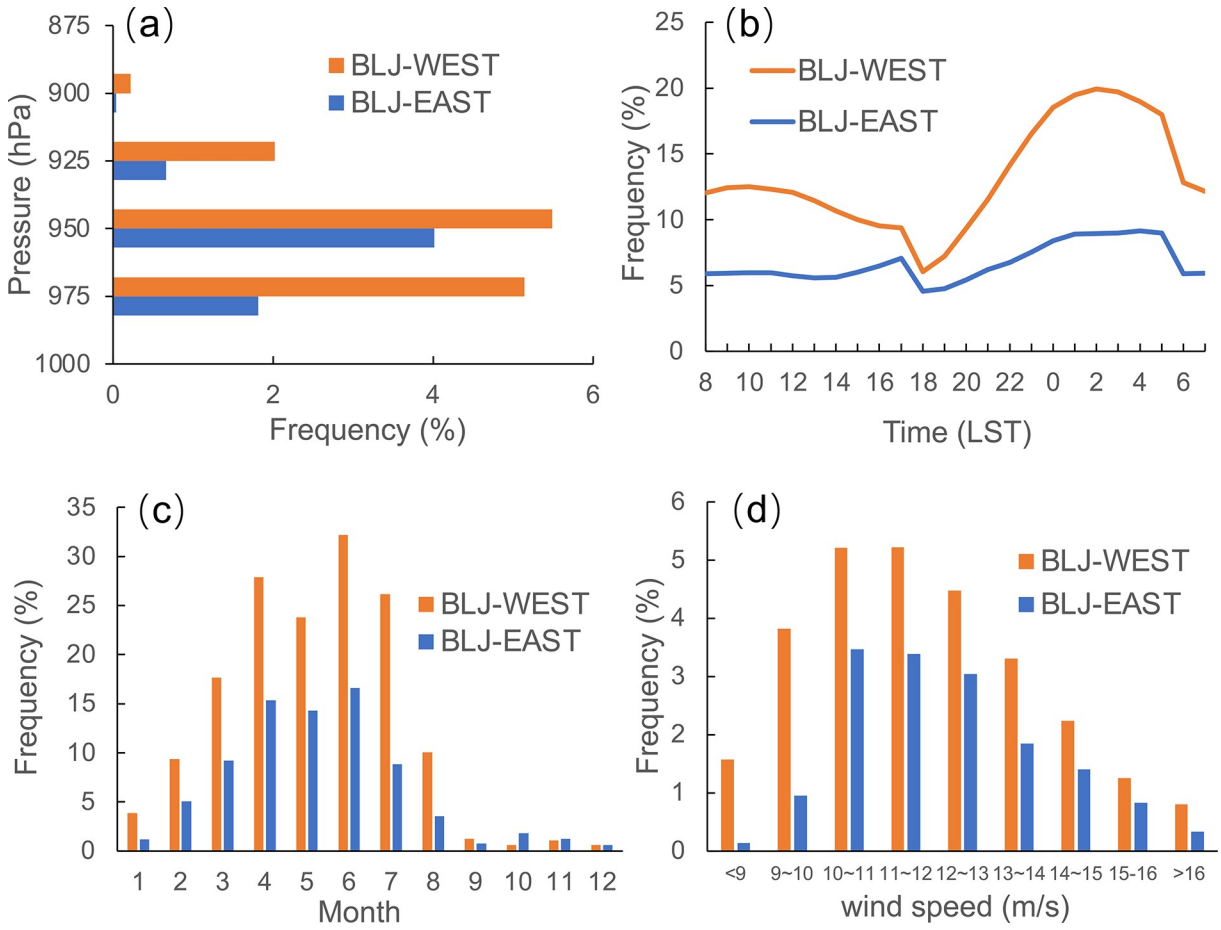

Fig. 2. (a) Vertical occurrence frequency distribution of BLJ cores for BLJ-WEST and BLJ-EAST events. (b) Diurnal cycle and (c) seasonal variation of BLJ-WEST and BLJ-EAST event occurrence frequency during Jan–Dec 1998–2018. (d) Histogram distribution of wind speed at 950 hPa averaged over boxes A and B for BLJ-WEST and BLJ-EAST events, respectively.

and f). The wind maximum cores at 950 hPa over the Beibu Gulf and the NSCS (Figs. 3c and 3e) correspond to high occurrence frequencies of the two CMBLJs (Fig. 1b). During the BLJ-WEST events, the wind core over the Beibu Gulf (~12 m s^{-1}) is stronger than that over the NSCS (~10 m s^{-1}). On the other hand, southerly winds over the NSCS (12 m s^{-1}) become strong during the BLJ-EAST events while strong winds prevail over the Beibu Gulf (~12 m s^{-1}) as well. These results suggest that the two CMBLJs are not completely independent and are related with each other.

3.2. *Relationship between the BLJ-WEST and the BLJ-EAST*

As shown in Fig. 4a, the occurrence frequency of the BLJ-WEST (24%) is higher than that of the BLJ-EAST (13%) during the early-summer rainy season. Interestingly, the simultaneous occurrence frequency of BLJ-WEST and BLJ-EAST events (BLJ-WEST-EAST events) is particularly high (~ 9.1%), which accounts for the majority of BLJ-EAST events. These results suggest that the BLJ-EAST is typically accompanied by the BLJ-WEST. Figure 4b presents the scatter diagram of 950-hPa wind speed averaged over the CMBLJs' core regions during the BLJ-WEST, the BLJ-EAST, and the BLJ-WEST-EAST events. The linear regressions of wind speeds for the two CMBLJs and their simultaneous occurrence show high correlations (R=0.63, 0.59, and 0.50 for the BLJ-WEST, BLJ-EAST, and BLJ-WEST-EAST events, respectively), which further confirms a close relationship between the BLJ-WEST and the BLJ-EAST and implies that both CMBLJs are controlled by the same large-scale environment (e.g., monsoon flows) but with different intensity of monsoonal airflow. When the airflow is strong, the BLJ-EAST and BLJ-WEST tend to appear together; when the airflow is weak, only the BLJ-WEST occurs. Therefore, the BLJ-EAST events show higher wind speeds extending more eastward compared to the BLJ-WEST (Fig. 3). Since the two CMBLJs may convey different thermodynamic features derived from their different upstream regions (e.g., Indochina Peninsula or South China Sea), it is necessary to examine their varying effect on rainfall in South China.

4. Rainfall associated with CMBLJs

The spatial distributions of rainfall associated with the two CMBLJs (BLJ-WEST and BLJ-EAST) are examined

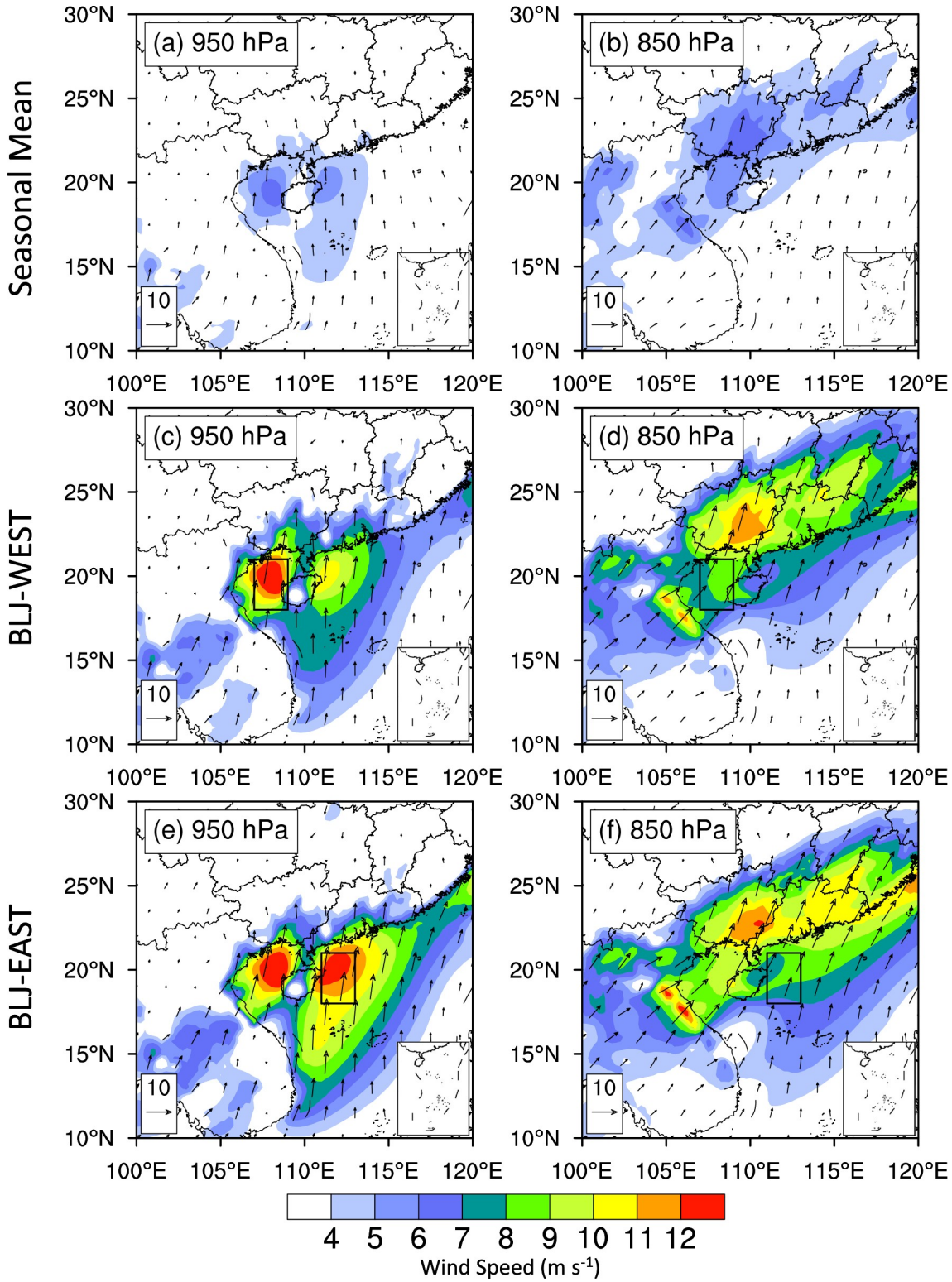

Fig. 3. Distribution of horizontal winds (m s^{-1}) at (a, c, and e) 950 hPa and (b, d, and f) 850 hPa for (a and b) the seasonal mean, (c and d) BLJ-WEST events, and (e and f) BLJ-EAST events during the early-summer rainy season.

compared to the seasonal rainfall mean. Figure 5a shows the climatological horizontal distribution of rainfall during the early-summer rainy season (April–June). Four main rainfall maximum centers (>0.4 mm h^{-1}) occur over northeastern Guangxi (Region L1), central Guangdong (Region L2), northern Fujian (Region L3), and Yangjiang (Region C2). An additional minor rainfall maximum center (~0.35 mm h^{-1}) is observed in Shanwei (Region C3). The rainfall centers agree well with surface observations (Luo et al., 2017).

During the BLJ-WEST or BLJ-EAST events, all the rain-

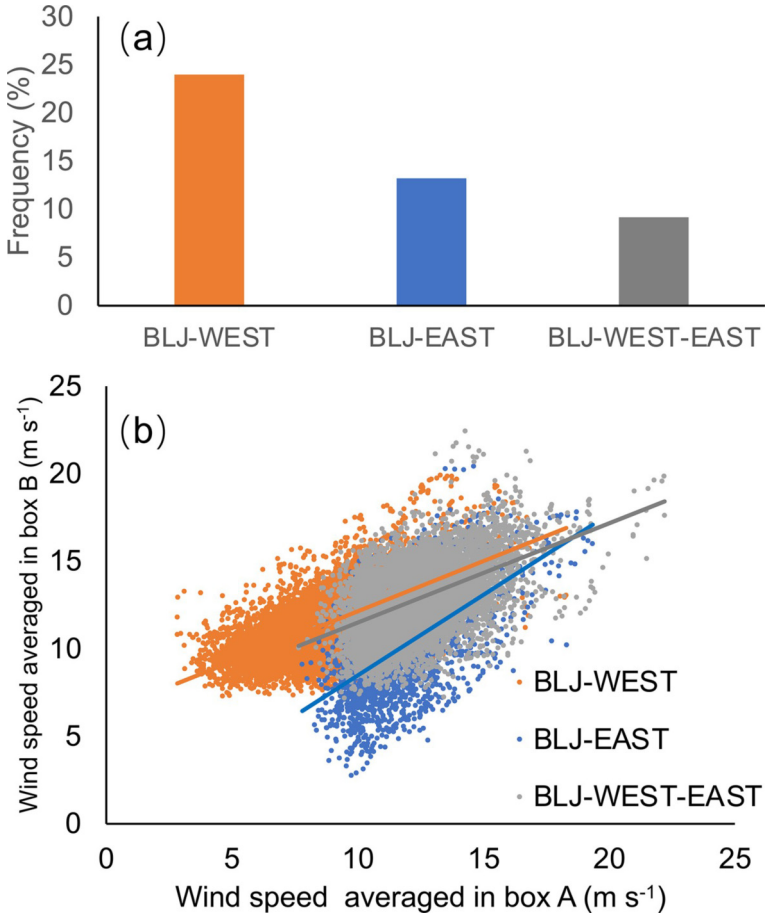

Fig. 4. (a) Occurrence frequency of BLJ-WEST, BLJ-EAST, and BLJ-WEST-EAST events during the early-summer rainy season. (b) Scatter diagram of wind speed at 950 hPa averaged over boxes A and B in Fig. 1b during BLJ-WEST, BLJ-EAST, and BLJ-WEST-EAST events.

fall centers are significantly strengthened compared to the seasonal mean (Figs. 5b and c). The rainfall intensity over Region L1 (~0.8 mm h^{-1}) is larger than that over Region L2 (~0.6 mm h^{-1}) during the BLJ-WEST events (Fig. 5b), whereas the rainfall over Region L2 (~1 mm h^{-1}) becomes stronger than that over Region L1 (~0.9 mm) during the BLJ-EAST events (Fig. 5c). The enhanced rainfall is closely linked to the strengthened low-level winds of the BLJ-WEST or BLJ-EAST. The influences of the two CMBLJs on rainfall exhibit their similarities and differences. Next, we will discuss the detailed impact mechanisms from dynamic and thermodynamic perspectives.

4.1. *Dynamical effects*

From a dynamic perspective, Fig. 6 compares the vertical cross sections of upward motion and meridional winds along lines a–c of Fig. 5 during the early-summer rainy season, the BLJ-WEST events, and the BLJ-EAST events. Compared to the seasonal mean, the vertical motion is strengthened near the coasts and on the windward side of mountains along with the enhancement of the BLJ-WEST or BLJ-EAST (Fig. 6). During the BLJ-WEST or BLJ-EAST events, strong CMBLJs peaking at 950–975 hPa impinge on the coastal terrain, which induces evident ascent with a center of 925 hPa near the coasts, including the south coast of Guangxi (Region C1) and the southwest and southeast coasts of Guangdong (Regions C2 and C3). Additionally, the CMBLJs extend further to the north at higher levels due to the locations of their maximum winds being tilted with height, and these winds impinge farther inland, reaching higher mountains, and produce elevated mesoscale ascent due to the CMBLJs' termini and terrain-induced lifting (Fu et al., 2019). As a result, significant 850-hPa vertical motion centers occur on the windward side of Yun-Gui Plateau (Region L1), Nanling mountain (Region L2), and Wuyi mountain (28°N, 118°E, Region L3), which are near the termini of the CMBLJs. The intensified upward motion is consistent with the enhanced low-level convergence and/or moisture flux convergence related to the CMBLJs and their interaction with coasts or terrain (Fig. 7). The upward motion averaged during the BLJ-EAST events (Figs. 6c, f, and i) is slightly stronger (~0.05 Pa s^{-1}) than that in the BLJ-WEST events (Figs. 6b, e, and h) because of stronger CMBLJs in the BLJ-EAST events (Fig. 3), resulting in more rainfall over South China in the BLJ-EAST events (Fig. 5c).

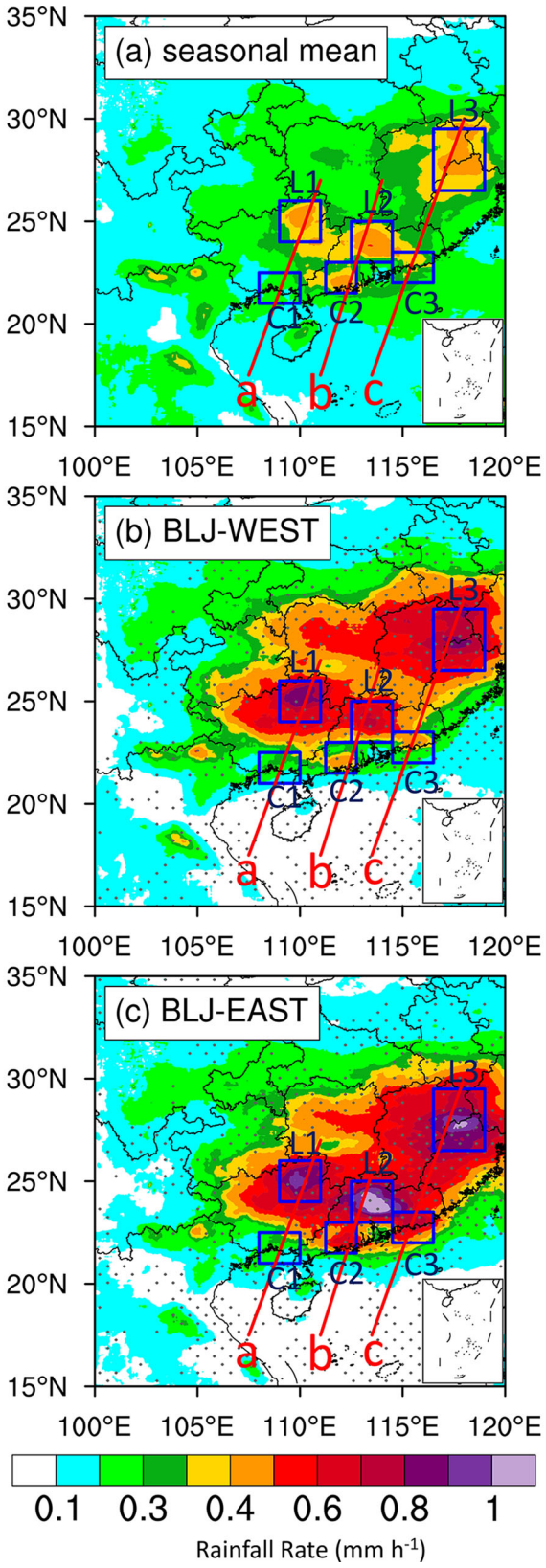

Fig. 5. Distribution of average rainfall rate (mm h^{-1}) for (a) the seasonal mean, (b) BLJ-WEST events, and (c) BLJ-EAST events during the early-summer rainy season. The dots in (b and c) denote the area where the significance level of the difference of rainfall between BLJ-WEST and BLJ-EAST is greater than 90% by two-tailed Welch's test.

4.2. *Thermodynamical effects*

Apart from dynamical effects, rainfall can also be influenced by the thermodynamic processes of the CMBLJs. The horizontal distributions of CAPE and CIN under the effect of the CMBLJs are shown in Fig. 8. The CAPE and CIN shown here are most unstable CAPE (MUCAPE) and surfaced-based CIN, respectively, which are directly obtained from the ERA5 dataset. In the seasonal mean, large CAPE occurs over the NSCS with a maximum of 2000 J kg^{-1} to the south of Hainan Island (~17°N, 110°E, Fig. 8a) because of abundant warm moist low-level airflow from the ocean. The large CAPE is transported by low-level southerlies to the north, with two branches surrounding Hainan Island, and reaches Regions C1 and C2, respectively. During BLJ-WEST events, more CAPE (~600 J kg^{-1}) is induced by warm moist air advection toward Region C1 and Region C2, with stronger high-CAPE branches (Fig. 8c). The branch of high CAPE to the east of Hainan Island becomes more significant during the BLJ-EAST events compared to the west branch (Fig. 8c vs Fig. 8e). Therefore, the CAPE production induced by warm moist air advection accompanied by CMBLJs enhances rainfall near the coastal areas (Regions C1 and C2). On the other hand, climatological CIN is relatively large over the Beibu Gulf (~200–300 J kg^{-1}), with a maximum of ~400 J kg^{-1} along the downstream side (northeast) of the Annamite Range (Fig. 8b). When stronger winds prevail and pass over the Annamite Range during the BLJ-WEST or BLJ-EAST events, higher CIN (~150 or 200 J kg^{-1}) occurs downstream of the Annamite Range (Figs. 8d and 8f), which mainly affects Region C1. Therefore, high CIN caused by the CMBLJs induces unfavorable conditions for coastal rainfall in the region. The CMBLJs induce stronger convergence in both Regions C1 and C2 but cause higher CIN in Region C1, which probably results in weaker rainfall in Region C1 compared to Region C3.

Next, we explain why high CIN is observed downstream of the Annamite Range (over the Beibu Gulf). In the lee of the mountain, isentropic surfaces are depressed and characterized by a hydraulic jump (Fig. 9a), which results in smaller temperature lapse rates at low levels (Fig. 10a). In addition, relative humidity at 950 hPa along the lee of the mountain is anomalously low (Fig. 10b) due to adiabatic heating (Fig. 9a). The two effects indicated above may jointly contribute to anomalously large CIN values in the lee of the mountain (Fig. 8b), which is consistent with the results from using an idealized model found by Markowski and Dotzek (2011). When the CMBLJs occur, the two effects become more significant (Figs. 9b and 10c–f) and thus yield larger CIN values in the lee of the mountain (Figs. 8d and f).

4.3. *Rainfall with varying CMBLJ intensity*

We further examine the variations of the rainfall patterns along with CMBLJ intensity. The CMBLJs are classified into four categories based on the wind speed of the CMBLJ core averaged over region A or B of Fig. 1b. Weak, moderate, strong, and extremely strong CMBLJs are

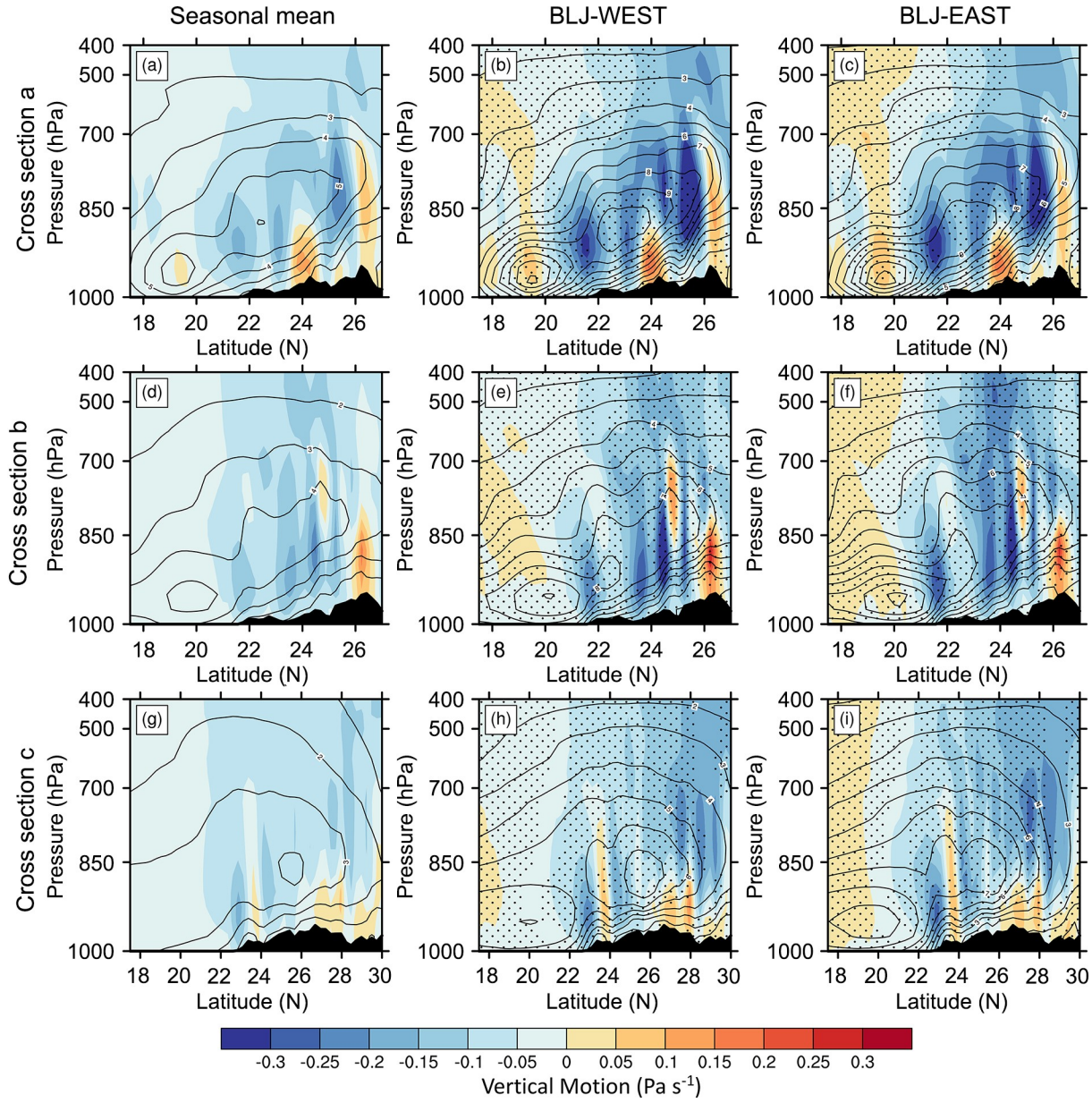

Fig. 6. Vertical cross section of vertical motion (shading, Pa s^{-1}) and meridional wind speed (contour with interval of 1 m s^{-1}) along (a–c) line a, (d–f) line b, and (g–i) line c in Fig. 5 for (a, d, and g) the seasonal mean or during the (b, e, and h) BLJ-WEST events and (c, f, and i) BLJ-EAST events during the early-summer rainy season. The dots denote the region where the significance level of the difference of vertical motion between BLJ-WEST and BLJ-EAST is greater than 90% by two-tailed Welch's test. The black shading indicates the terrain.

defined when the wind speed at 950 hPa of the CMBLJ core is less than 11 m s^{-1}, between 11 m s^{-1} and 13 m s^{-1}, between 13 m s^{-1} and 15 m s^{-1}, and greater than 15 m s^{-1}, respectively. Figure 2d shows the histogram distribution of wind speeds at 950 hPa for the BLJ-WEST and BLJ-EAST. Most of CMBLJs are identified as weak or moderate (10–13 m s^{-1}). There are enough samples representing these four categories. We also classify groups using different percentiles instead of the fixed threshold, and the results are consistent with the fixed thresholds. Since the wind speed threshold of 15 m s^{-1} is located at around the 92nd percentile, the fourth category (>15 m s^{-1}) represents extremely strong CMBLJs.

The horizontal distributions of rainfall under the effect of the BLJ-WESTs or BLJ-EASTs are shown in Fig. 11. As we expected, the rainfall rates over the inland regions (Regions L1–L3) increase along with CMBLJ intensity. In particular, the enhanced BLJ-WEST tends to increase rainfall more over Region L1 compared to Regions L2 and L3 (Figs. 11a, c, e, and g), while the enhanced BLJ-EAST tends to increase rainfall more over Regions L2 and L3 (Figs. 11b, d, f, and g). However, the variation of coastal rainfall associated with CMBLJ intensity is complicated compared to the variation of inland rainfall. Coastal rainfall in

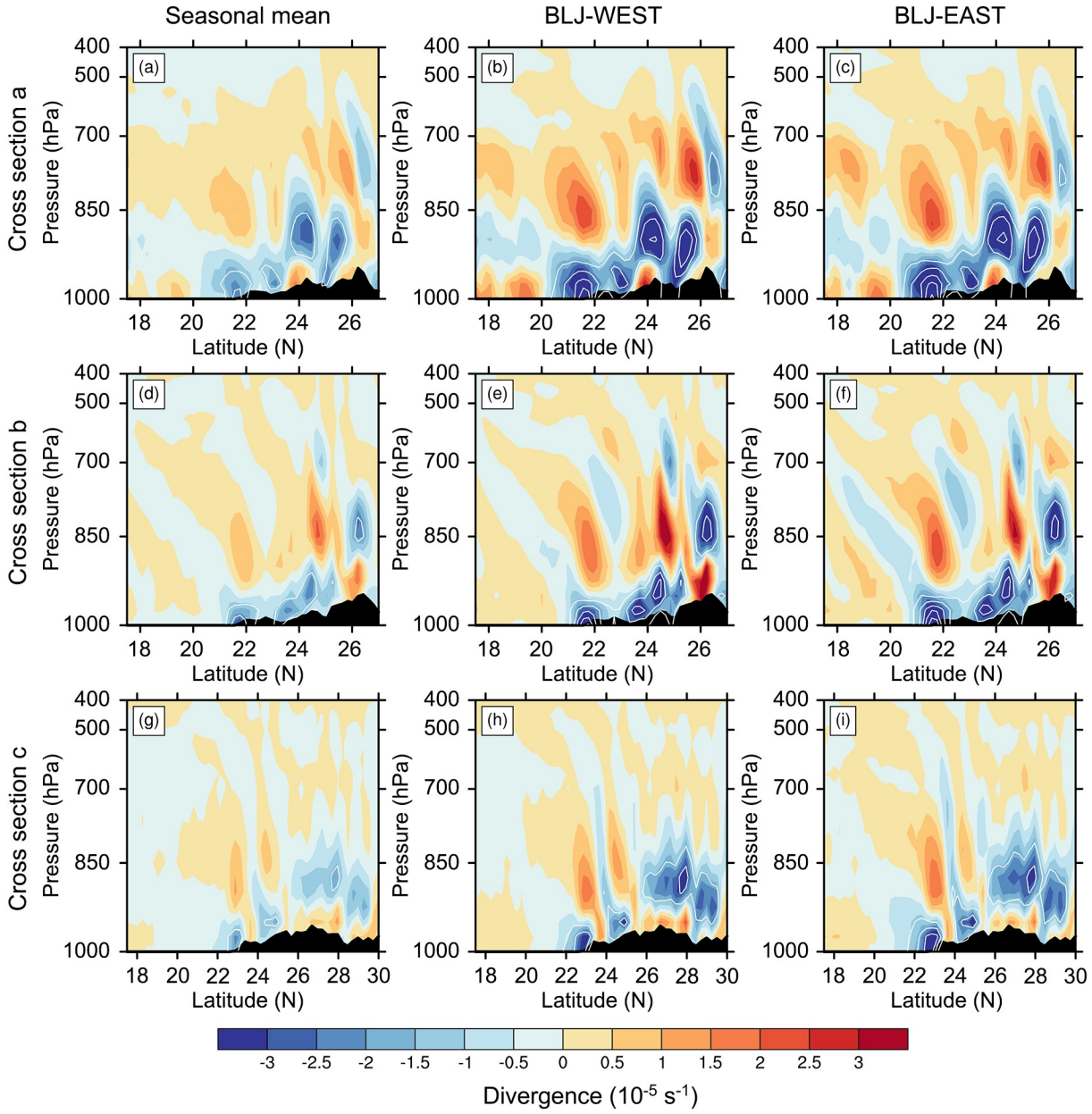

Fig. 7. Vertical cross section of divergence (shading, s^{-1}) and moisture flux divergence (white contour $\leq -2 \times 10^{-7}$ kg kg^{-1} s^{-1} with interval of 2×10^{-7} kg kg^{-1} s^{-1}) along (a–c) line a, (d–f) line b, and (g–i) line c in Fig. 5 for (a, d, and g) the seasonal mean or during the (b, e, and h) BLJ-WEST events and (c, f, and i) BLJ-EAST events during the early-summer rainy season. The black shading indicates the terrain.

Regions C1 and C2 becomes strongest during strong BLJ-WEST events (Fig. 11e) rather than extremely strong BLJ-WEST events (Fig. 11g). Similarly, rainfall in Region C2 peaks during moderate BLJ-EAST events. In contrast, coastal rainfall in Region C3 increases along with the intensity of the BLJ-WEST or BLJ-EAST, which resembles the behavior of inland rainfall but differs from the other coastal rainfall centers.

Figure 12 further confirms the detailed variation of rainfall at different locations with CMBLJs of different intensities. Except for Regions C1 and C2 (black and dark blue bars of Fig. 12), most Regions (L1–3, and C3) have rainfall intensities that undergo nearly continuous increases with increasing CMBLJ intensity.

Next, we explore the causes of non-monotone rainfall variations with CMBLJ intensity in Regions C1 and C2. Figure 13 shows the response of vertical motion to the varying CMBLJs interacting with coasts and terrain. In addition to locations upstream of inland mountains, upward motion is maximized at around 950 hPa near the coastal areas due to the convergence at the termini of the CMBLJs and the induction by the variation in land–sea roughness (Fig. 13). With the enhancement of the CMBLJs, coastal lifting is strengthened accordingly, which is consistent with the vari-

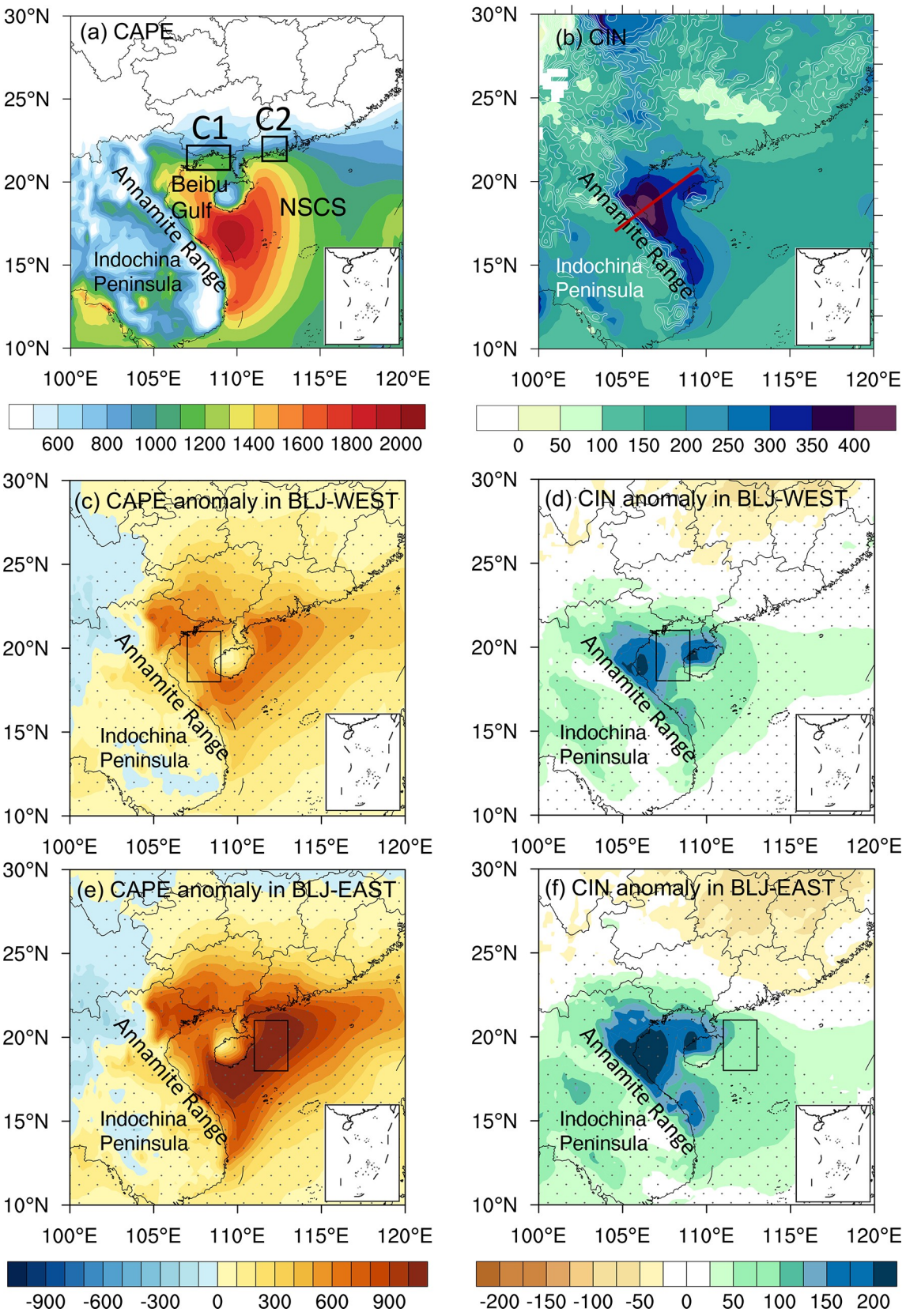

Fig. 8. Horizontal distributions of (a) CAPE (J kg^{-1}) and (b) CIN (J kg^{-1}) during the early-summer rainy season. The differences in (c) CAPE and (d) CIN between the BLJ-WEST events and the seasonal mean. The differences in (e) CAPE and (f) CIN between BLJ-EAST events and the seasonal mean. The dots in (c–f) denote the area where the significance level of the difference of CAPE/CIN between BLJ-WEST and BLJ-EAST is greater than 90% by two-tailed Welch's test.

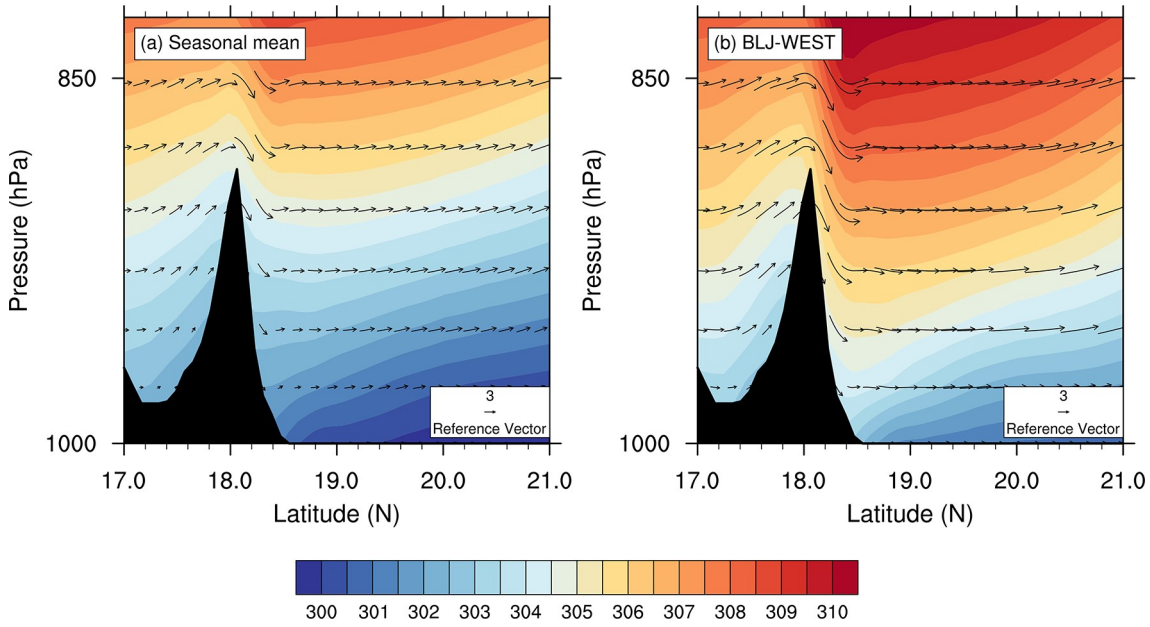

Fig. 9. Vertical cross section along the red line in Fig. 8b of potential temperature (shading, K) and flow vectors (m s^{-1}, black curly vector along the cross section and with vertical velocity amplified by 200) for (a) the seasonal mean or during (b) the BLJ-WEST events of the early-summer rainy season. The black shading indicates the terrain.

ation of inland topographic lifting. In addition, stronger moisture flux convergence is produced by stronger CMBLJs (Fig. 13). However, the strongest coastal lifting and moisture flux convergence among the four categories do not result in the most rainfall in Regions C1 and C2 from the perspective of dynamics, which implies that thermodynamic processes might play an important role.

The variation of CIN along with CMBLJ intensity is further examined (Fig. 14). It clearly shows that CIN near Regions C1 and C2 becomes higher with stronger CMBLJs (Fig. 14). This happens because CIN is enhanced downstream of the Annamite Range and is accompanied with stronger southwesterly flow (Fig. 9), which is confirmed by Markowski and Dotzek (2011). The other possible reason is that surface temperature is reduced (CIN thus increases) over the Indochina Peninsula at night when the CMBLJs are strengthened, and CIN over the Beibu Gulf is increased by cold and dry air over the Indochina Peninsula being transported downstream by the southwesterly flow.

We also examine the variation of CAPE along with CMBLJ intensity. The moderate (strong) BLJ-WEST produces larger CAPE in Regions C1–C3 than the weak (moderate) BLJ-WEST (Figs. 15a and 15b) since more warm moist air is transported by stronger southerly flow from the South China Sea. When the BLJ-WEST strengthens further (from strong to extremely strong), CAPE in Region C1 is instead reduced because cold and dry air is transported from the Indochina Peninsula to influence the Beibu Gulf (Fig. 15c). In terms of BLJ-EASTs, a similar variation of CAPE with CMBLJ intensity occurs (Figs. 15d–f). The strong (extremely strong) BLJ-EAST results in lower CAPE in Regions C1 and C2 compared to the moderate (strong) BLJ-EAST (Figs. 15e and 15f). CAPE over the Indochina Peninsula becomes lower at night due to the radiation cooling near the surface when the BLJ over the Indochina Peninsula (land) is strengthened, owing to inertial oscillation.

To further confirm that smaller CAPE is induced by cold and dry air being transported from the Indochina Peninsula to the Beibu Gulf under the action of a stronger CMBLJ, we calculate the budget of CAPE generation in the diurnal cycle (Fig. 16). Since the CMBLJ becomes stronger at night, we mainly compare the nighttime and daytime horizontal advection. Figure 16a shows that CAPE at 950 hPa increases at the coast of the Beibu Gulf, by around 40–80 J kg^{-1} at 0200 LST. The CAPE at 950 hPa is computed from lifting the parcel at the source pressure of 950 hPa rather than at the surface. We chose 950 hPa as the base level to calculate CAPE because the jet peaks at around 950 hPa and influences the transportation of warm moist air associated with CAPE changes. It is noted that CAPE at 950 hPa has estimation errors in the inland region due to terrain height, but we mainly focus on the CAPE over the ocean and coastal area in the present study.

The CAPE change is mainly caused by boundary layer forcing (Fig. 16b), while free-tropospheric forcing generates a relatively small CAPE change over both the ocean and the land (Fig. 16c). As mentioned in section 2, boundary layer forcing can be further divided into horizontal advection, vertical lifting, and external diabatic heating (Figs. 16d–f). Figure 16d shows that vertical lifting can enhance CAPE by more than 240 J kg^{-1} at the coastal area. The warm and humid air in the lower layer is uplifted by terrain along the coastal area, which leads to the increase of convective instability (CAPE thus increases). Because of nocturnal radiation cooling near the surface, equivalent potential temperature over the Indochina Peninsula becomes lower at night (Fig.

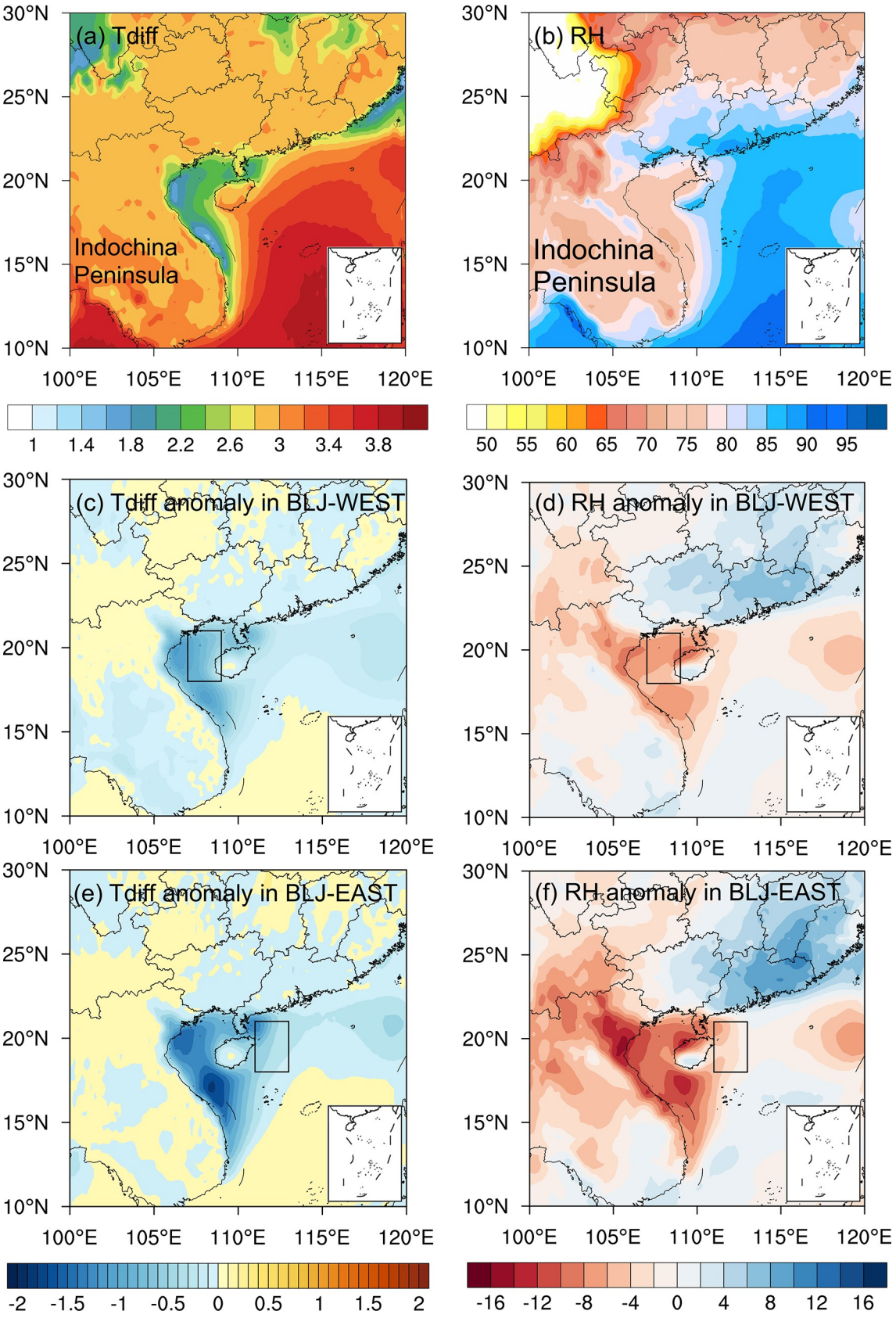

Fig. 10. Distribution of (a) temperature difference between 1000 hPa and 950 hPa (Tdiff, units: K) and (b) relative humidity (RH) at 950 hPa during the early-summer rainy season. The differences in (b) Tdiff and (e) RH between BLJ-WEST events and the seasonal mean. The differences in (c) Tdiff and (f) RH between BLJ-EAST events and the seasonal mean.

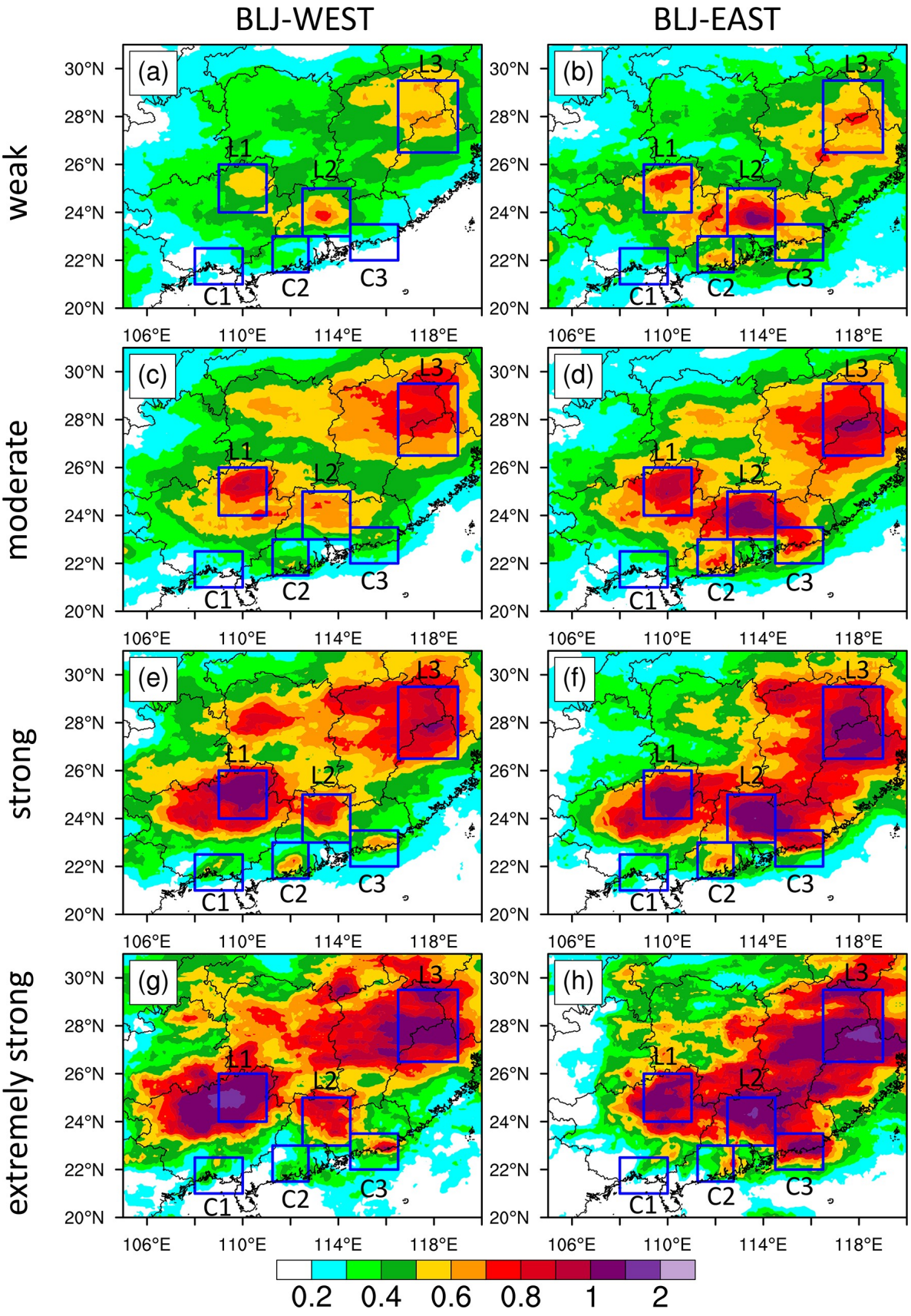

Fig. 11. Distribution of average rainfall rate (mm h^{-1}) for (a and b) weak, (c and d) moderate, (e and f) strong, and (g and h) extremely strong (a, c, e, and g) BLJ-WEST events and (b, d, f, and h) BLJ-EAST events during the early-summer rainy season.

16g). Horizontal advection brings relatively cold and dry air from the Indochina Peninsula to the Beibu Gulf, leading to a decrease of the warm and wet energy in the boundary layer over the Beibu Gulf, and thus contributes negatively toward CAPE generation by about –200 J kg^{-1} (Fig. 16e). Comparing the patterns at 0200 LST and 1400 LST (Figs. 16e and 16h), the CAPE reduction due to the horizontal advection is more significant over the Beibu Gulf at night when the CMBLJ is more intense.

Therefore, the stronger CMBLJ transports the cold and dry air from the Indochina Peninsula to the Beibu Gulf more quickly, resulting in a greater decrease of warm and wet energy in the boundary layer and thus contributes more negatively toward CAPE generation, which can offset the CAPE generation contributed by coastal dynamic lifting. As a result, the decrease of CAPE generation inhibits the development of convection and weakens the nighttime precipitation of the western coast.

5. Summary

In the present study, 21 years of hourly ERA5 reanalysis and CMORPH satellite rainfall data are used to investigate the characteristics of coastal marine boundary layer jets (CMBLJs) near the south coast of China and their impacts on coastal and inland rainfall over South China. The CMBLJ frequency distribution indicates two main branches of southerly CMBLJs, one on either side of Hainan Island: one over the Beibu Gulf (BLJ-WEST) and one over the NSCS (BLJ-EAST). The two CMBLJs peak at around 950 hPa and exhibit significant seasonal variations with maximums in the pre-summer rainy season (April–June). Similar

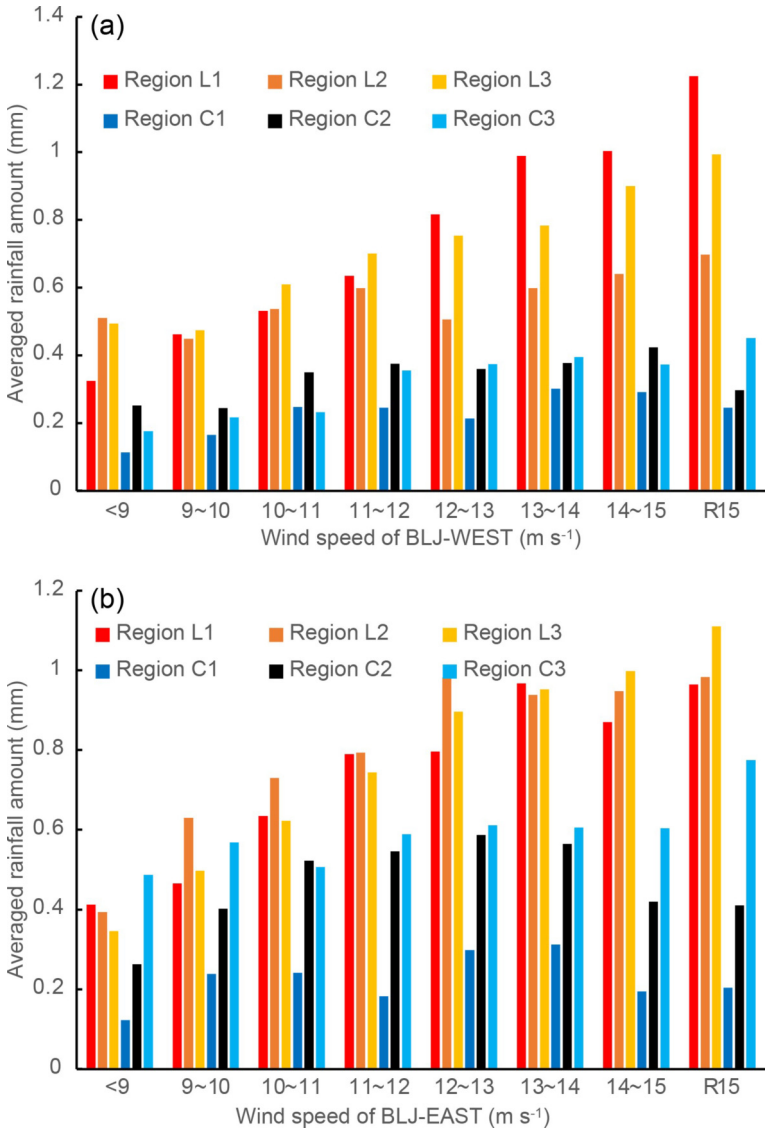

Fig. 12. Histogram distribution of rainfall amount (mm) averaged in Regions L1–L3 and C1–C3 for different intensities of (a) BLJ-WEST and (b) BLJ-EAST (represented by wind speed at 950 hPa averaged over boxes A and B in Fig. 1b).

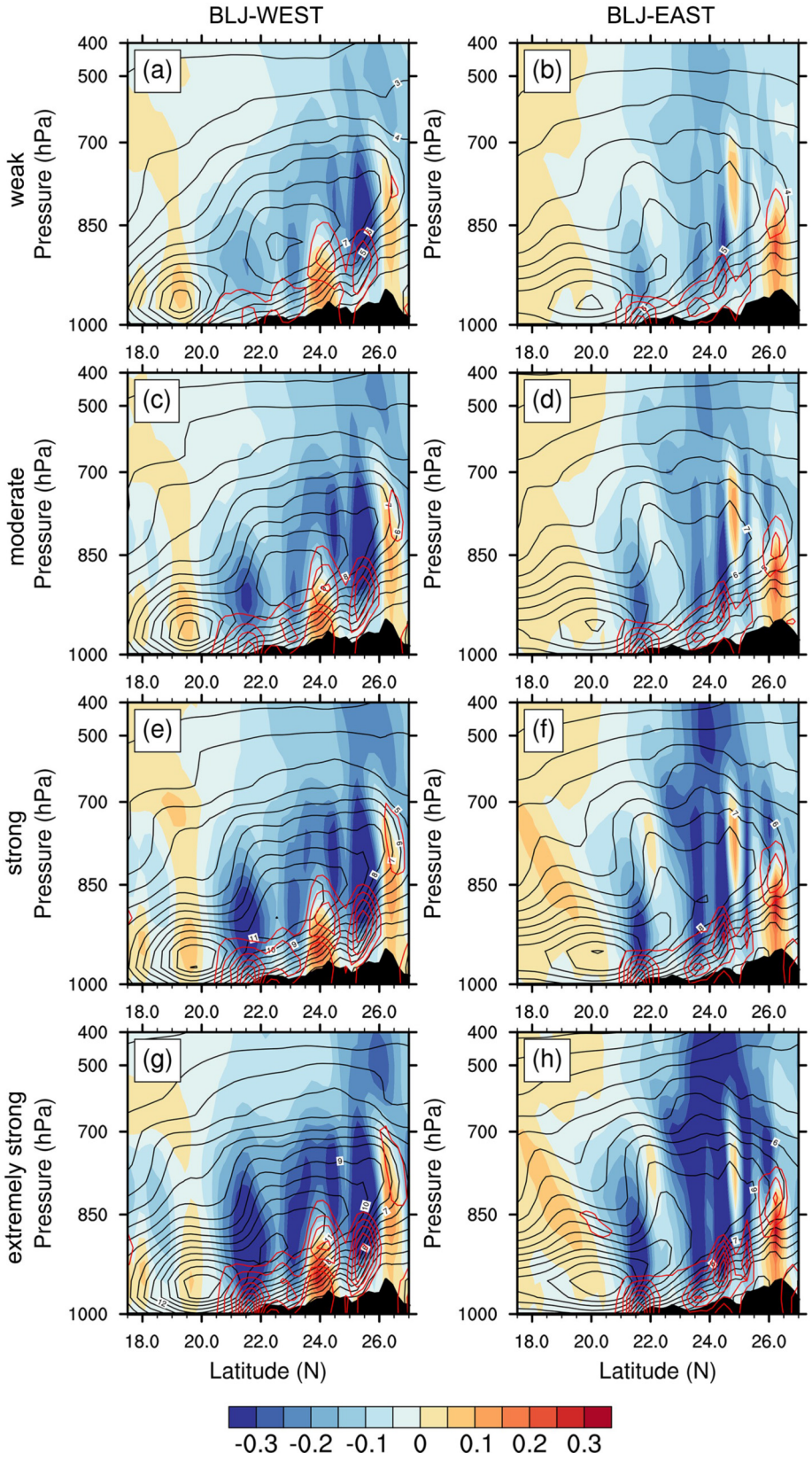

Fig. 13. Vertical cross section of vertical motion (shading, Pa s^{-1}), meridional wind speed (black contour with interval of 1 m s^{-1}), and horizontal moisture flux divergence (red contour, $\leq -2 \times 10^{-7}$ kg kg^{-1} s^{-1} with interval of 2×10^{-7} kg kg^{-1} s^{-1}) along (a, c, e, and g) line a and (b, d, f, and h) line b in Fig. 5 during the BLJ-WEST events and BLJ-EAST events, respectively.

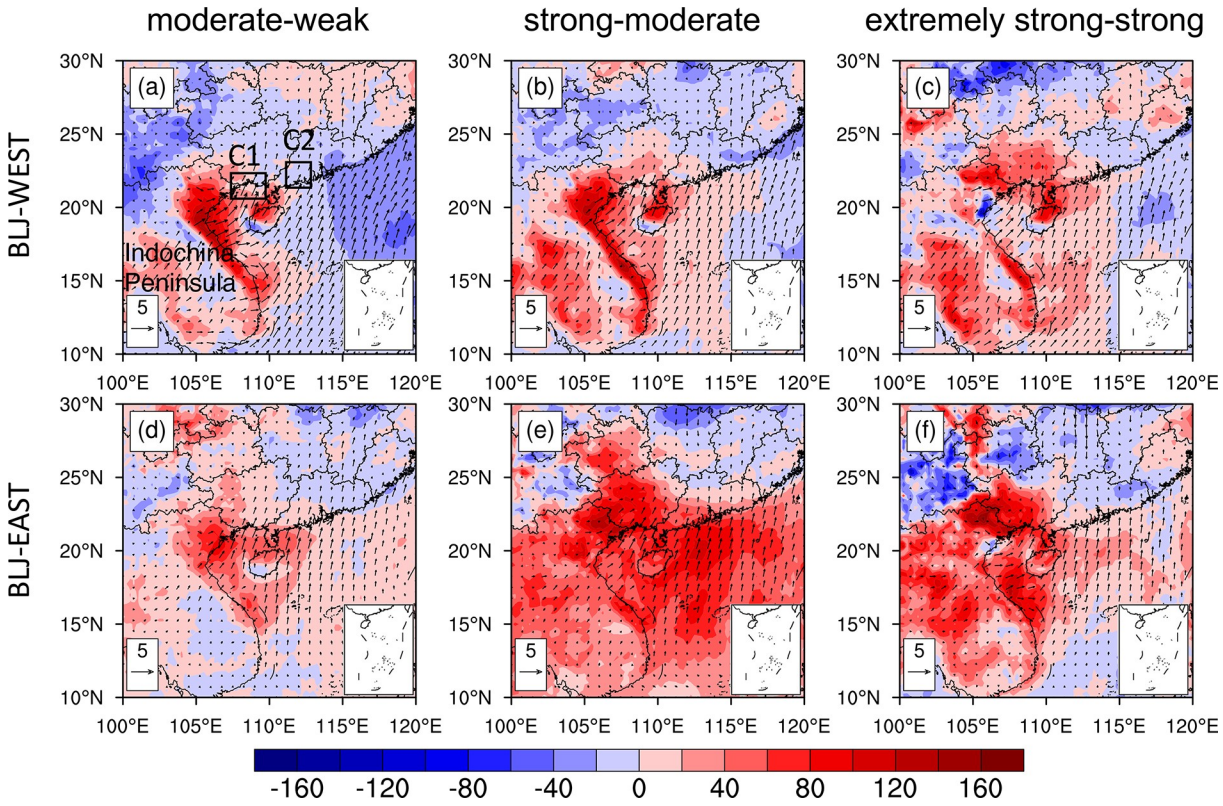

Fig. 14. Differences in CIN (J kg^{-1}) and wind vectors (m s^{-1}) at 950 hPa between (a) moderate and weak BLJ-WEST events, between (b) strong and moderate BLJ-WEST events, and between very strong and strong BLJ-WEST events. (d–f) Same as (a–c) except for BLJ-EAST events.

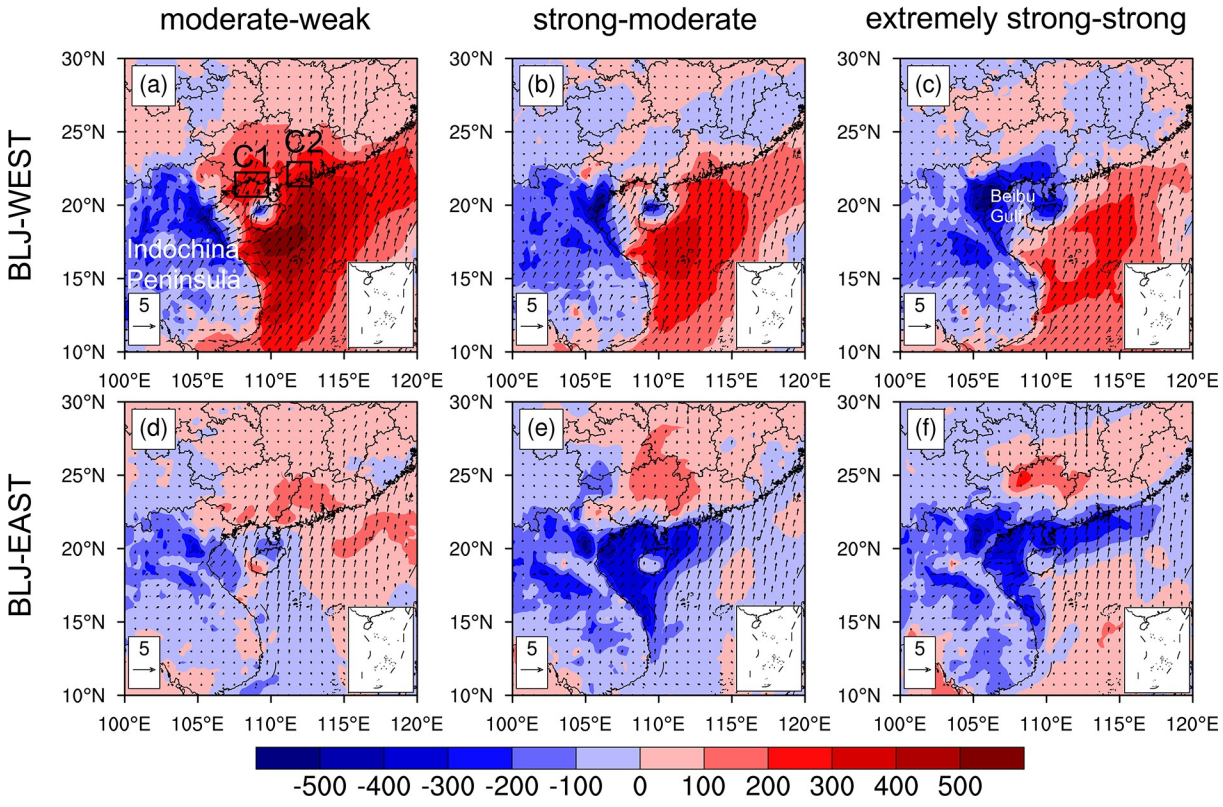

Fig. 15. Differences in CAPE (J kg^{-1}) and wind vectors (m s^{-1}) at 950 hPa between (a) moderate and weak BLJ-WEST events, between (b) strong and moderate BLJ-WEST events, and between (c) very strong and strong BLJ-WEST events. (d–f) Same as (a–c) except for BLJ-EAST events.

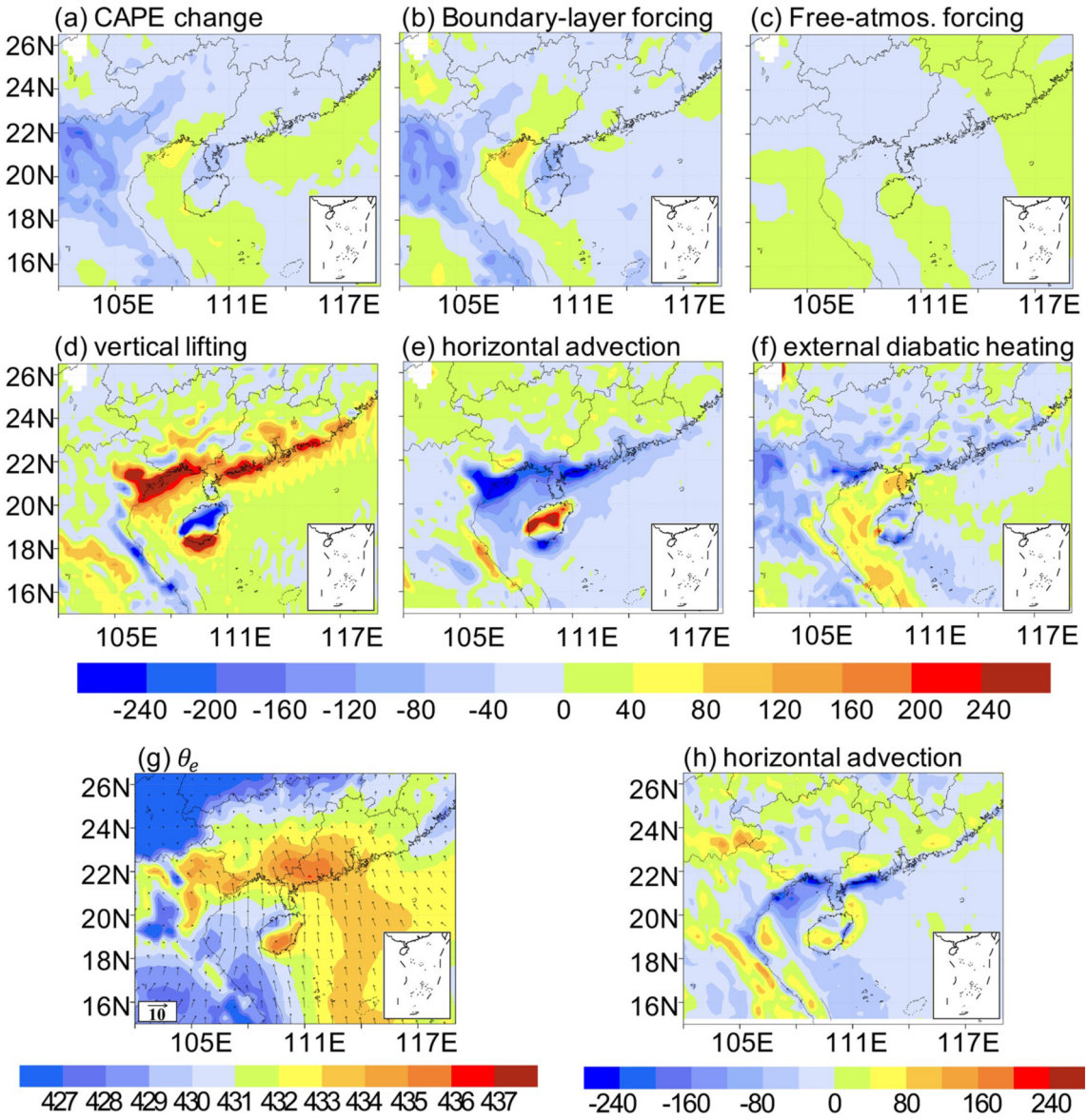

Fig. 16. Distribution of (a) the CAPE change (units: J kg^{-1} h^{-1}) at 950 hPa at 0200 LST averaged during the early-summer rainy season and (b–f) the CAPE generation rates (units: J kg^{-1} h^{-1}) by various physical processes. Distribution of (g) equivalent potential temperature θ_e (K) at 950 hPa at 0200 LST and (h) the CAPE changes (units: J kg^{-1} h^{-1}) attributable to the horizontal advection term at 950 hPa at 1400 LST.

to boundary layer jets over the inland part of South China (Du et al., 2014), the two CMBLJs are both strongest at midnight (~0200–0500 LST). The two CMBLJs are not independent each other and always strengthen together.

The two CMBLJs show a close relationship with rainfall in South China. Coastal and inland rainfall is significantly enhanced when the two CMBLJs occur. The BLJ-WEST tends to intensify rainfall downstream in northern Guangxi, while the BLJ-EAST tends to intensify rainfall in central Guangdong and western and eastern coastal Guangdong (Yangjiang and Shanwei). The enhanced rainfall is mainly attributed to the lifting due to the convergence in the terminus of the CMBLJ or terrain-induced lifting interacting with the CMBLJ flow. CAPE changes induced by warm moist air advection from the NSCS to coastal or inland areas by the CMBLJs are another favorable condition for enhanced rainfall. Compared to coastal Guangdong, rainfall near coastal Guangxi is much weaker because of higher CIN in the Beibu Gulf downstream of the Annamite Range. In the lee of the mountain, depressed isentropic surfaces decrease the temperature lapse rate at low levels, while adiabatic heating reduces relative humidity. These two effects jointly contribute to anomalously large CIN in the Beibu Gulf.

Dynamic lifting and anomalous CAPE and CIN associated with the CMBLJs jointly result in anomalous rainfall. The inland rainfall nearly continuously increases along with CMBLJ intensity because of stronger dynamic lifting and stronger CAPE production induced by warm moist air advection under the effect of stronger CMBLJs. In contrast, the rela-

tionship between CMBLJ intensity and coastal rainfall does not show a positive correlation, except for rainfall near Shanwei. Coastal rainfall reaches a maximum when moderate or strong CMBLJs occur, rather than extremely strong CMBLJs. The non-monotone rainfall variations with CMBLJ intensity are attributed to the combination of favorable and unfavorable factors along with CMBLJ intensity. With the intensification of the CMBLJs, dynamic lifting is enhanced (favorable condition) but CIN becomes higher (unfavorable condition). In addition, CAPE over the coastal area increases with an enhancement of the CMBLJs due to the warm and humid air uplifted by terrain-induced lifting. However, CAPE in the coastal areas of Guangxi and Yangjiang is further reduced under extremely strong CMBLJs because of the negative contribution of CAPE generation caused by the horizontal advection of cold and dry air from the Indochina Peninsula offsetting the CAPE generation contributed by coastal dynamic lifting.

In the future, it is necessary to examine CMBLJ activities using offshore observations from scientific research ships to compare with the results of reanalysis. Higher resolution WRF simulations are required to explore the CMBLJ features and mechanisms in details. Recently, Kong et al. (2020) documented that the BLJ-WEST is mainly driven by an upstream continental nocturnal LLJ crossing over the Annamite Range of Vietnam, associated with a hydraulic jump and topography blocking effects near Hainan Island. However, the cause of another CMBLJ high occurrence region located east of Hainan Island is not well understood and needs to be further studied. The influence of the CMBLJs on rainfall intensity is addressed in the present study, but the detailed effects of the CMBLJs on coastal and inland convection initiation and development should be clarified, from a climatological perspective, in the future.

Acknowledgements. This paper is dedicated to and in memory of Professor Fuqing ZHANG who was one of the world's leaders on mesoscale meteorology. His passion for scientific research inspired our early-career scientists. This study was supported by the National Key Research and Development Program of China (Grant No. 2018YFC1507402), the National Natural Science Foundation of China (Grant Nos. 42122033, 41875055, 42075006, and 41861164027), Guangzhou Science and Technology Plan Projects (202002030346 and 202002030196), and the Young Elite Scientists Sponsorship Program by CAST (2018QNRC001).

REFERENCES

Amador, J. A., V. O. Magaña, and J. B. Pérez, 2000: The low level jet and convective activity in the Caribbean. Preprints, *24th Conf. on Hurricanes and Tropical Meteorology*, Fort Lauderdale, FL, American Meteorological Society, 114–115.

Blackadar, A. K., 1957: Boundary layer wind maxima and their significance for the growth of nocturnal inversions. *Bull. Amer. Meteor. Soc.*, **38**, 283–290, https://doi.org/10.1175/1520-0477-38.5.283.

Bonner, W. D., 1968: Climatology of the low level jet. *Mon. Wea. Rev.*, **96**, 833–850, https://doi.org/10.1175/1520-0493(1968)096<0833:COTLLJ>2.0.CO;2.

Burk, S. D., and W. T. Thompson, 1996: The summertime low-level jet and marine boundary layer structure along the California coast. *Mon. Wea. Rev.*, **124**(4), 668–686, https://doi.org/10.1175/1520-0493(1996)124<0668:TSLLJA>2.0.CO;2.

Chakraborty, A., R. S. Nanjundiah, and J. Srinivasan, 2009: Impact of African orography and the Indian summer monsoon on the low-level Somali jet. *International Journal of Climatology*, **29**, 983–992, https://doi.org/10.1002/joc.1720.

Chen, G. T. J., and C. C. Yu, 1988: Study of low-level jet and extremely heavy rainfall over northern Taiwan in the Mei-Yu season. *Mon. Wea. Rev.*, **116**, 884–891, https://doi.org/10.1175/1520-0493(1988)116<0884:SOLLJA>2.0.CO;2.

Chen, G. X., R. Yoshida, W. M. Sha, T. Iwasaki, and H. L. Qin, 2014: Convective instability associated with the eastward-propagating rainfall episodes over eastern China during the warm season. *J. Climate*, **27**(6), 2331–2339, https://doi.org/10.1175/JCLI-D-13-00443.1.

Chen, G. X., W. M. Sha, T. Iwasaki, and Z. P. Wen, 2017a: Diurnal cycle of a heavy rainfall corridor over East Asia. *Mon. Wea. Rev.*, **145**(8), 3365–3389, https://doi.org/10.1175/MWR-D-16-0423.1.

Chen, X. C., F. Q. Zhang, and K. Zhao, 2017b: Influence of monsoonal wind speed and moisture content on intensity and diurnal variations of the Mei-Yu season coastal rainfall over south China. *J. Atmos. Sci.*, **74**, 2835–2856, https://doi.org/10.1175/JAS-D-17-0081.1.

Chen, G. X., R. Y. Lan, W. X. Zeng, H. Pan, and W. B. Li, 2018: Diurnal variations of rainfall in surface and satellite observations at the monsoon coast (South China). *J. Climate*, **31**(5), 1703–1724, https://doi.org/10.1175/JCLI-D-17-0373.1.

Chen, G. X., Y. Du, and Z. P. Wen, 2021: Seasonal, interannual, and interdecadal variations of the East Asian summer monsoon: A diurnal-cycle perspective. *J. Climate*, **34**(11), 4403–4421, https://doi.org/10.1175/JCLI-D-20-0882.1.

Chen, Y.-L., X. A. Chen, and Y.-X. Zhang, 1994: A diagnostic study of the low-level jet during TAMEX IOP 5. *Mon. Wea. Rev*, **122**, 2257–2284, https://doi.org/10.1175/1520-0493(1994)122<2257:ADSOTL>2.0.CO;2.

Doubler, D. L., J. A. Winkler, X. D. Bian, C. K. Walters, and S. Y. Zhong, 2015: An NARR-derived climatology of southerly and northerly low-level jets over North America and coastal environs. *J. Appl. Meteorol. Climatol.*, **54**(7), 1596–1619, https://doi.org/10.1175/JAMC-D-14-0311.1.

Du, Y., and R. Rotunno, 2014: A simple analytical model of the nocturnal low-level jet over the great plains of the United States. *J. Atmos. Sci.*, **71**, 3674–3683, https://doi.org/10.1175/JAS-D-14-0060.1.

Du, Y., and G. X. Chen, 2018: Heavy rainfall associated with double low-level jets over Southern China. *Part I: Ensemble-based analysis. Mon. Wea. Rev.*, **146**, 3827–3844, https://doi.org/10.1175/MWR-D-18-0101.1.

Du, Y., and G. X. Chen, 2019a: Heavy rainfall associated with double low-level jets over Southern China. *Part II: Convection initiation. Mon. Wea. Rev.*, **147**, 543–565, https://doi.org/10.1175/MWR-D-18-0102.1.

Du, Y., and G. X. Chen, 2019b: Climatology of low-level jets and their impact on rainfall over southern China during the early-summer rainy season. *J. Climate*, **32**, 8813–8833, https://doi.org/10.1175/JCLI-D-19-0306.1.

Du, Y., Q. H. Zhang, Y. L. Chen, Y. Y. Zhao, and X. Wang, 2014: Numerical simulations of spatial distributions and diurnal variations of low-level jets in China during early summer. *J. Climate*, **27**, 5747–5767, https://doi.org/10.1175/JCLI-D-13-00571.1.

Du, Y., Y.-L. Chen, and Q. H. Zhang, 2015: Numerical simulations of the boundary layer jet off the southeastern coast of China. *Mon. Wea. Rev.*, **143**, 1212–1231, https://doi.org/10.1175/MWR-D-14-00348.1.

Emanuel, K. A., 1994: *Atmospheric Convection*. Oxford University Press, 580 pp.

Fu, P. L., K. F. Zhu, K. Zhao, B. W. Zhou, and M. Xue, 2019: Role of the nocturnal low-level jet in the formation of the morning precipitation peak over the Dabie Mountains. *Adv. Atmos. Sci.*, **36**, 15–28, https://doi.org/10.1007/s00376-018-8095-5.

Garreaud, R., and R. C. Muñoz, 2005: The low-level jet off the west coast of subtropical South America: Structure and variability. *Mon. Wea. Rev.*, **133**(8), 2246–2261, https://doi.org/10.1175/MWR2972.1.

Holton, J. R., 1967: The diurnal boundary layer wind oscillation above sloping terrain. *Tellus*, **19**, 199–205, https://doi.org/10.1111/j.2153-3490.1967.tb01473.x.

Jiang, Q. F., S. P. Wang, and L. O'Neill, 2010: Some insights into the characteristics and dynamics of the Chilean low-level coastal jet. *Mon. Wea. Rev.*, **138**, 3185–3206, https://doi.org/10.1175/2010MWR3368.1.

Joyce, R. J., J. E. Janowiak, P. A. Arkin, and P. P. Xie, 2004: CMORPH: A method that produces global precipitation estimates from passive microwave and infrared data at high spatial and temporal resolution. *Journal of Hydrometeorology*, **5**, 487–503, https://doi.org/10.1175/1525-7541(2004)005<0487:CAMTPG>2.0.CO;2.

Kalverla, P. C., J. B. Duncan Jr., G. J. Steeneveld, and A. A. M. Holtslag, 2019: Low-level jets over the North Sea based on ERA5 and observations: Together they do better. *Wind Energy Science*, **4**(2), 193–209, https://doi.org/10.5194/wes-4-193-2019.

Kong, H., Q. H. Zhang, Y. Du, and F. Zhang, 2020: Characteristics of coastal low-level jets over Beibu gulf, China, during the early warm season. *J. Geophys. Res.: Atmos.*, **125**, e2019JD031918, https://doi.org/10.1029/2019JD031918.

Krishnamurti, T. N., J. Molinari, and H. L. Pan, 1976: Numerical simulation of the Somali jet. *J. Atmos. Sci.*, **33**, 2350–2362, https://doi.org/10.1175/1520-0469(1976)033<2350:NSOTSJ>2.0.CO;2.

Li, J., and Y. L. Chen, 1998: Barrier jets during TAMEX. *Mon. Wea. Rev.*, **126**, 959–971, https://doi.org/10.1175/1520-0493(1998)126<0959:BJDT>2.0.CO;2.

Li, X., and Y. Du, 2021: Statistical relationships between two types of heavy rainfall and low-level jets in South China. *J. Climate*, **34**, 8549–8566, https://doi.org/10.1175/JCLI-D-21-0121.1.

Liu, W. R., K. H. Cook, and E. K. Vizy, 2020: Role of the West African westerly jet in the seasonal and diurnal cycles of precipitation over West Africa. *Climate Dyn.*, **54**(1–2), 843–861, https://doi.org/10.1007/s00382-019-05035-1.

Luo, Y., and Coauthors, 2017: The Southern China monsoon rainfall experiment (SCMREX). *Bull. Amer. Meteor. Soc.*, **98**, 999–1013, https://doi.org/10.1175/BAMS-D-15-00235.1.

Marengo, J. A., W. R. Soares, C. Saulo, and M. Nicolini, 2004: Climatology of the low-level jet east of the Andes as derived from the NCEP–NCAR reanalyses: Characteristics and temporal variability. *J. Climate*, **17**(12), 2261–2280, https://doi.org/10.1175/1520-0442(2004)017<2261:COTLJE>2.0.CO;2.

Markowski, P. M., and N. Dotzek, 2011: A numerical study of the effects of orography on supercells. *Atmospheric Research*, **100**, 457–478, https://doi.org/10.1016/j.atmosres.2010.12.027.

Neiman, P. J., F. M. Ralph, A. B. White, D. E. Kingsmill, and P. O. G. Persson, 2002: The statistical relationship between upslope flow and rainfall in California's coastal mountains: Observations during CALJET. *Mon. Wea. Rev.*, **130**(6), 1468–1492, https://doi.org/10.1175/1520-0493(2002)130<1468:TSRBUF>2.0.CO;2.

Rife, D. L., J. O. Pinto, A. J. Monaghan, C. A. Davis, and J. R. Hannan, 2010: Global distribution and characteristics of diurnally varying low-level jets. *J. Climate*, **23**, 5041–5064, https://doi.org/10.1175/2010JCLI3514.1.

Shapiro, A., E. Fedorovich, and S. Rahimi, 2016: A unified theory for the Great Plains nocturnal low-level jet. *J. Atmos. Sci.*, **73**, 3037–3057, https://doi.org/10.1175/JAS-D-15-0307.1.

Smith, B. L., S. E. Yuter, P. J. Neiman, and D. E. Kingsmill, 2010: Water vapor fluxes and orographic precipitation over northern California associated with a landfalling atmospheric river. *Mon. Wea. Rev.*, **138**, 74–100, https://doi.org/10.1175/2009MWR2939.1.

Stensrud, D. J., 1996: Importance of low-level jets to climate: A review. *J. Climate*, **9**, 1698–1711, https://doi.org/10.1175/1520-0442(1996)009<1698:IOLLJT>2.0.CO;2.

Tao, S., and L. Chen, 1987: *A Review of Recent Research on the East Asian Summer Monsoon in China*. *Oxford University Press*, 60–92.

Tu, C. C., Y. L. Chen, P. L. Lin, and Y. Du, 2019: Characteristics of the marine boundary layer jet over the South China Sea during the early summer rainy season of Taiwan. *Mon. Wea. Rev.*, **147**, 457–475, https://doi.org/10.1175/MWR-D-18-0230.1.

White, A. B., P. J. Neiman, F. M. Ralph, D. E. Kingsmill, and P. O. G. Persson, 2003: Coastal orographic rainfall processes observed by radar during the California Land-Falling Jets Experiment. *Journal of Hydrometeorology*, **4**(2), 264–282, https://doi.org/10.1175/1525-7541(2003)4<264:CORPOB>2.0.CO;2.

Whyte, F. S., M. A. Taylor, T. S. Stephenson, and J. D. Campbell, 2008: Features of the Caribbean low level jet. *International Journal of Climatology*, **28**(1), 119–128, https://doi.org/10.1002/joc.1510.

Zhang, F., Q. H. Zhang, Y. Du, and H. Kong, 2018: 2018: Characteristics of coastal low-level jets in the Bohai Sea, China, during the early warm season. *J. Geophys. Res.: Atmos.*, **123**(24), 13 763–13 774, https://doi.org/10.1029/2018JD029242.

Zhang, G. J., 2002: Convective quasi-equilibrium in midlatitude continental environment and its effect on convective parameterization. *J. Geophys. Res.: Atmos.*, **107**, 4220, https://doi.org/10.1029/2001JD001005.

Zhang, M. R., and Z. Y. Meng, 2018: Impact of synoptic-scale factors on rainfall forecast in different stages of a persistent heavy rainfall event in South China. *J. Geophys. Res.: Atmos.*, **123**, 3574–3593, https://doi.org/10.1002/2017JD028155.